ACS OMEGA

http://pubs.acs.org/journal/acsodf

Article

Non-antimicrobial and Non-anticancer Properties of ZnO Nanoparticles Biosynthesized Using Different Plant Parts of *Bixa orellana*

Saee Gharpure, Rachana Yadwade, and Balaprasad Ankamwar*

Cite This: *ACS Omega* 2022, 7, 1914−1933

Read Online

ACCESS | Metrics & More | Article Recommendations | Supporting Information

ABSTRACT: As traditional cancer therapy is toxic to both normal and cancer cells, there is a need for newer approaches to specifically target cancer cells. ZnO nanoparticles can be promising due their biocompatible nature. However, ZnO nanoparticles have also shown cytotoxicity against mammalian cells in some cases, because of which there is a need for newer synthesis approaches for biocompatible ZnO nanoparticles to be used as carrier molecules in drug delivery applications. Here, we report the biosynthesis of ZnO nanoparticles using different plant parts (leaf, seed, and seed coat) of *Bixa orellana* followed by different characterizations. The UV−visible spectra of ZnO showed absorption maxima at 341 and 353 nm, 378 and 373 nm, and 327 and 337 nm, respectively, before and after calcination corresponding to the band gap energy of 3.636 and 3.513 eV, 3.280 and 3.324 eV, and 3.792 and 3.679 eV for L-ZnO, S-ZnO, and Sc-ZnO, respectively. X-ray diffraction analysis confirmed the formation of hexagonal wurtzite structures. Attenuated total reflectance infrared spectra revealed the presence of stretching vibrations of C−C, C═C, C═O, and NH_3^+ groups along with C−H deformation involving biomolecules from extracts responsible for reduction and stabilization of nanoparticles. Field emission scanning electron microscopy and transmission electron microscopy images showed spherical and almond-like morphologies of L-ZnO and Sc-ZnO with spherical morphologies, whereas S-ZnO showed almond-like morphologies. The presence of antibacterial activity was observed in L-ZnO against *Staphylococcus aureus* and *Bacillus subtilis*, in S-ZnO nanoparticles only against *Escherichia coli*, and in Sc-ZnO only against *Staphylococcus aureus*. Uncalcinated ZnO nanoparticles showed weak antibacterial activities, whereas calcinated ZnO nanoparticles showed a non-antibacterial nature. The antifungal activity against different fungi (*Penicillium* sp., *Aspergillus flavus*, *Fusarium oxysporum*, and *Rhizoctonia solani*) and cytotoxicity against HCT-116 cancer cells were not observed before and after calcination in all three ZnO nanoparticles. The antimicrobial nature and biocompatibility of ZnO nanoparticles were influenced by different parameters of the nanoparticles along with microorganisms and the human cells. Non-antimicrobial properties of ZnO nanoparticles can be treated as a pre-requisite for its biocompatibility due to its inert nature. Thus, biosynthesized ZnO nanoparticles showed a nontoxic nature, which can be exploited as promising alternatives in biomedical applications.

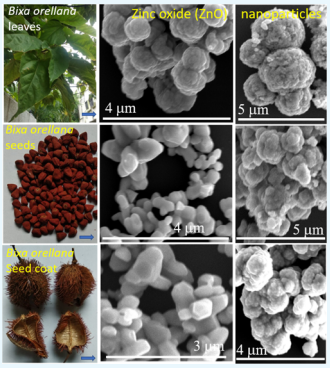

1. INTRODUCTION

In recent times, the World Health Organization has stated microbial antibiotic resistance to be among the most critical crises faced by humans. Microbial infections have gained a lot of attention due to its serious health hazards. New bacterial mutation, antibiotic resistance, outbreaks of pathogenic strains, and so forth, have been increasing at an alarming rate because of which the effective antimicrobials are the need of the time.[1,2] There has been ever increasing demand for development of novel anti-microbial agents due to incidence of microbial infections. These causative agents cannot be treated by traditional antibiotics due to newly developed antimicrobial resistance which has been a serious issue.[3,4] Nanoparticles can be considered to be potential antimicrobial agents due to their excellent activity against surface contamination, adhesion, and colonization which are detrimental for the human health.[5] Metal and metal oxide nanoparticles such as silver, gold, copper, iron oxide, titanium oxide, zinc oxide, and so forth, have shown antimicrobial properties at very low concentration by virtue of their unique physicochemical properties. Some of these metal-based nanoparticles have shown a biocompatible nature against human cells and even serve as micronutrients essential for vital functioning of the human body.[6]

Zinc is among the micronutrients which are required by the human body for its vital functioning as it is required for activity of various enzymes such as carbonic anhydrase, carboxypeptidase, and alcohol dehydrogenase, which are important in eukaryotic metabolic activities.[7] Zinc oxide (ZnO), a widely studied metal oxide, shows a 3.37 eV band gap energy and 60

Received: September 25, 2021
Accepted: December 27, 2021
Published: January 5, 2022

https://doi.org/10.1021/acsomega.1c05324
ACS Omega 2022, 7, 1914−1933

eV excitation energy along with being considered to be "generally recognized as safe (GRAS)" according to the US-FDA.[8] ZnO nanoparticles are well-known for their antimicrobial properties against various microorganisms because of which these nanoparticles have been exploited in different fields such as food science, cosmetics, agriculture, medicine, and pharmaceuticals.[9] Even though the exact mechanism responsible for these activities is not completely known, generation of reactive oxygen species (ROS) is majorly responsible for both antibacterial and antifungal properties.[10,11] There are several reports showing that the interaction of ZnO nanoparticles with bacterial cells results in structural changes of the microbial cell membrane, thereby triggering cytoplasmic leakage and ultimately resulting in cell death.[12] Action of ZnO nanoparticles on fungal cells has been observed to cause deformation of hyphae as a result of uncontrolled accumulation of cellular components, interference with cellular function resulting in cell death.[13,14] In addition to its antimicrobial activities, ZnO nanoparticles have also been used in drug delivery applications.[15] However, there are also reports by the EU hazard classification which have classified zinc oxide as eco-toxic. Zinc compounds have been observed to be toxic for mammalian and plant systems in trace amounts.[16] Moreover, there are several reports which show cytotoxicity against human and animal cells due to oxidative stress and cellular damage caused by release of zinc ions, thereby limiting their use in biomedical applications.[17] Use of biocompatible ZnO nanoparticles in drug delivery applications is critical as it can be used in alternate therapy specifically targeting cancer cells and not normal cells. This may help overcome the drawbacks of traditional cancer treatments such as radiation therapy and chemotherapy, which show high levels of cytotoxicity against cancer and normal cells.[18,19] Thus, there is a need to focus attention on synthesizing ZnO nanoparticles which are non-toxic, ensuring that they will not elicit an immune response when administered into the human body. Use of these nanoparticles as "controlled release reservoirs" would in turn aid in targeted delivery of drugs, thereby facilitating a therapy against many diseases. Use of biocompatible ZnO nanoparticles in drug delivery applications will always be preferred over other inorganic nanoparticles as biodistribution studies show no adverse effects *in vivo*.[20,21] Previous reports have shown that the toxic nature of ZnO nanoparticles against different microorganisms and mammalian cells have been influenced by different physicochemical properties of nanoparticles such as size, morphology, surface coating, concentration, and so forth.[22] Toxicity of ZnO nanoparticles can also be contributed by its mode of synthesis. For example, physical and chemical methods have been reported to contribute to its toxic nature which in turn hampers its applicability.[23] Thus, there is a need for newer methods for synthesizing ZnO nanoparticles with unique physicochemical properties, high anti-microbial activities, and low cytotoxicity which can be suitable for different bio-applications.

There are several reports regarding different physical, chemical, and biological methods used for synthesizing zinc oxide nanoparticles.[24] However, physical and chemical methods used for synthesizing ZnO nanoparticles have associated disadvantages such as requirement of exact instrumentation, increased expenses, and use of hazardous chemicals which limit their widespread use in various applications.[25] Due to these reasons, biosynthesis has been one of the most preferred methods for synthesizing ZnO which makes use of natural sources such as plants and plant parts, bacteria, fungi and biomacromolecules for reduction/oxidation of zinc precursors thus acting as capping and stabilizing agents.[26] Also, functionalization of ZnO nanoparticles with biomolecules has been observed to contribute to their biocompatibility by decreasing their cytotoxicity against human cells because of which it has been a widely preferred approach.[27] There are several reports where ZnO nanoparticles have been synthesized using different plant parts such as leaf of *Agathosma betulina*, fruit of *Calotropis procera*, bulb of *Petroselinum crispum*, bark of *Boswellia ovalifoliolata*, milk of *Carica papaya*, flower of *Nyctanthes arbortristis*, and so forth which have been further employed for various applications.[28] However, fewer studies have been performed using different parts of the same plant in the synthesis of ZnO nanoparticles.[29] Also, the use of different parts from the plant source *Bixa orellana* for synthesizing ZnO nanoparticles have not been reported yet. It will be interesting to study the role of different biomolecules from the same plant source in ZnO biosynthesis, its physicochemical properties, and influence on different bio-applications.

B. orellana L. which is a part of the Bixaceae family is a high bush of height 3 m. It is also known as Annatto and is grown in humid tropical climate conditions principally in the Central and Southern America. Extracts from different plants parts have been used for preventing several ailments such as constipation, ulcers, high fever, asthma, skin diseases, infectious diseases, allergies, and so on. Qualitative analysis of leaves, seeds, and seed coats have reported the presence of various phytochemicals such as carbohydrates, steroids, aromatics, terpenoids, tannins, saponins, essential oils, proteins, and so forth, thereby contributing to a wide range of pharmacological activities such as antimicrobial, antioxidant, anticancer, anti-inflammatory, anticonvulsant, analgesic, and antidiarrheal activities.[30] These phytochemicals present in extracts derived from leaves, seeds, and seed coats of *B. orellana* with different bioactivities act as reducing and stabilizing agents during the biosynthesis of zinc oxide nanoparticles which can be further exploited for various bio-applications.

Herein, we have reported the biosynthesis of zinc oxide nanoparticles using extracts from different parts such as leaves, seeds, and seed coats from the same plant, that is, *B. orellana* which act as reducing, capping and stabilizing agents followed by their characterization. Furthermore, estimation of antimicrobial activities using different bacteria (*Escherichia coli*, *Pseudomonas aeruginosa*, *Staphylococcus aureus*, *Bacillus subtilis*) and fungi (*Penicillium* sp., *Aspergillus flavus*, *Fusarium oxysporum*, *Rhizoctonia solani*) was performed followed by their cytotoxicity studies on cancer cell lines (human colorectal carcinoma cell line HCT-116).

2. RESULTS AND DISCUSSION

2.1. Biosynthesis of Zinc Oxide Nanoparticles. ZnO nanoparticles were biosynthesized with the help of leaf, seed, and seed coat extracts of *B. orellana* (L-ZnO, S-ZnO and Sc-ZnO) using 0.05 M zinc acetate as the zinc precursor salt. After addition of the extract and ammonia to 0.05 M zinc acetate solution, a pale yellow to brownish colored precipitate was observed. The addition of plant extracts to zinc acetate solution resulted in physicochemical changes in the reaction mixture. Among all the physicochemical changes, a color change was among the most prominent one which was

https://doi.org/10.1021/acsomega.1c05324
ACS Omega 2022, 7, 1914−1933

observed in a time period of few minutes upon addition of plant extracts. The change of the precipitate color from pale yellow to brownish was due to the coating with biomolecules from the extracts and was considered to be an initial signature for formation of ZnO nanoparticles. Naseer et al. reported ZnO biosynthesis using a *Cassia fistula* leaf extract which showed a color change from yellow to light brown thus signifying synthesis of ZnO nanoparticles.[31] In another study, Sadiq et al. have shown the color change from yellow to reddish brown thus confirming ZnO biosynthesis using *Syzygium cumini* leaves.[32] The biomolecules present in leaf, seed, and seed coat extracts of *B. orellana* (BL, BS and BSc) acted as reducing and stabilizing agents in bio-reduction of Zn^{2+} ions, thereby forming ZnO nanoparticles. The so-formed ZnO nanoparticles were further divided into two parts, one of which was calcined, whereas the other was air-dried. White-colored ZnO nanoparticles were obtained after calcination. Characterization of biosynthesized ZnO nanoparticles before and after calcination was further carried out using UV−vis spectrometry, photoluminescence (PL) studies, field emission scanning electron microscopy (FESEM), energy dispersive X-ray spectroscopy (EDS), transmission electron microscopy (TEM), X-ray diffraction (XRD), X-ray photoelectron spectroscopy (XPS), attenuated total reflectance infrared spectroscopy (ATR-IR), Brunauer, Emmett, Teller−Barrett, Joyner, Halenda (BET-BJH), gas chromatography−mass spectrometry (GC−MS), high resolution−mass spectrometry (HR-MS), and nuclear magnetic resonance (NMR) analysis.

2.2. Characterization of ZnO Nanoparticles.

2.2.1. UV−Visible Spectroscopic Analysis. UV−visible spectra were recorded within the interval of 300−1100 nm for ZnO nanoparticles before calcination (line 1), after calcination (line 2) and BL, BS, and BSc extracts (line 3) as represented in Figure 1. The influence of biomolecules from plant extracts contributing to bio-reduction of zinc ions to zinc oxide has been confirmed by signatures present in the UV−visible spectra. L-ZnO showed an absorption maxima at 341 and 353 nm, respectively, before and after calcination with 3.636 and 3.513 eV, respectively, as the corresponding band gap energies (Figure 1a). S-ZnO showed an absorption maxima at 378 and 373 nm, respectively, before and after calcination with 3.280 and 3.324 eV respectively as the corresponding band gap energies (Figure 1b). Similarly, Sc-ZnO showed an absorption maxima at 327 and 337 nm, respectively, before and after calcination with 3.792 and 3.679 eV, respectively, as the corresponding band gap energies (Figure 1c).

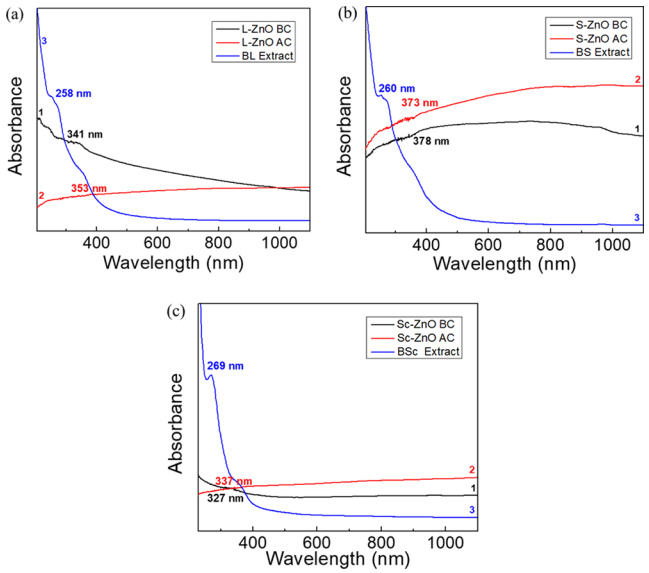

Figure 1. UV−vis absorption spectra of uncalcinated L-ZnO (line 1), calcined L-ZnO (line 2) and BL extract (line 3) (a), uncalcinated S-ZnO (line 1), calcined S-ZnO (line 2) and BS extract (line 3) (b) and uncalcinated Sc-ZnO (line 1), calcined Sc-ZnO (line 2) and BSc extract (line 3) (c)

Calculations of band gap energy have been carried out based upon the following equation

$$E_g = \frac{hc}{\lambda} = \frac{1240}{\lambda} \quad (1)$$

where h represents Planck's constant (4.136×10^{-15} eV•s), c represents the velocity of light (2.998×10^{8} m/s), and λ represents the cut off wavelength.

Kalpana et al. reported an absorption maxima of ZnO nanoparticles between the range 320−390 nm.[33] In another study, the successful biosynthesis of ZnO nanoparticles using the *Rubus fairholmianus* root extract has been observed to show an absorption maxima at 357 nm with band gap energy of 3.47 eV.[34] The absorption maxima of ZnO nanoparticles was also reported at 337 nm with band gap energy of 3.68 eV.[35] Thus, ZnO nanoparticles have shown an absorption maxima ∼370 nm with 3.35 eV band gap energy which is a characteristic of ZnO nanoparticles, thereby confirming its synthesis as reported in several other studies.[36] A typical absorption maxima present at ∼370 nm has been observed which can be attributed to the intrinsic band gap absorption of the ZnO as a result of the excitation of electrons from the valence band to the conduction band (O 2p → Zn 3d). Thus, all three ZnO nanoparticles show a high absorption coefficient in the UV region (<400 nm).[37] Also, the shift in the absorption maxima has been observed in ZnO nanoparticles before and after calcination due to various factors such as band gap, increase in quantum confinement, oxygen deficiencies, changes in size and morphology of nanoparticles, surface properties, and so forth.[38] BL, BS, and BSc extracts showed an absorption maxima between the range 260−270 nm which signifies presence of flavonoids, phenolics, and glycosides.[39] Thus, the biosynthesis of ZnO nanoparticles has been confirmed with the help of phytochemicals which majorly include phenolics, flavonoids, and glycosides which aid in the bio-reduction of zinc precursor salts.

2.2.2. PL Analysis. The PL study of ZnO nanoparticles before and after calcination is very important because they provide information about the properties of nanoparticles and their purity. The PL spectra of L-ZnO, S-ZnO and Sc-ZnO before and after calcination have been analyzed within the interval of 200−750 nm as represented in Figure 2. PL spectra of L-ZnO before calcination (line 1) showed peaks at 467 and 551 nm and that after calcination (line 2) showed peaks at 470 and 557 nm, respectively (Figure 2a). PL spectra of S-ZnO before calcination (line 1) showed peaks at 468 and 554 nm and that after calcination (line 2) showed peaks at 469 and 552 nm, respectively (Figure 2b). PL spectra of Sc-ZnO before calcination (line 1) showed peaks at 467 and 561 nm and that after calcination (line 2) showed peaks at 468 and 558 nm, respectively (Figure 2c). Previous studies show the excitation of ZnO nanoparticles over a wide range of wavelengths from near UV and blue light. PL spectra majorly showed two

https://doi.org/10.1021/acsomega.1c05324
ACS Omega 2022, 7, 1914−1933

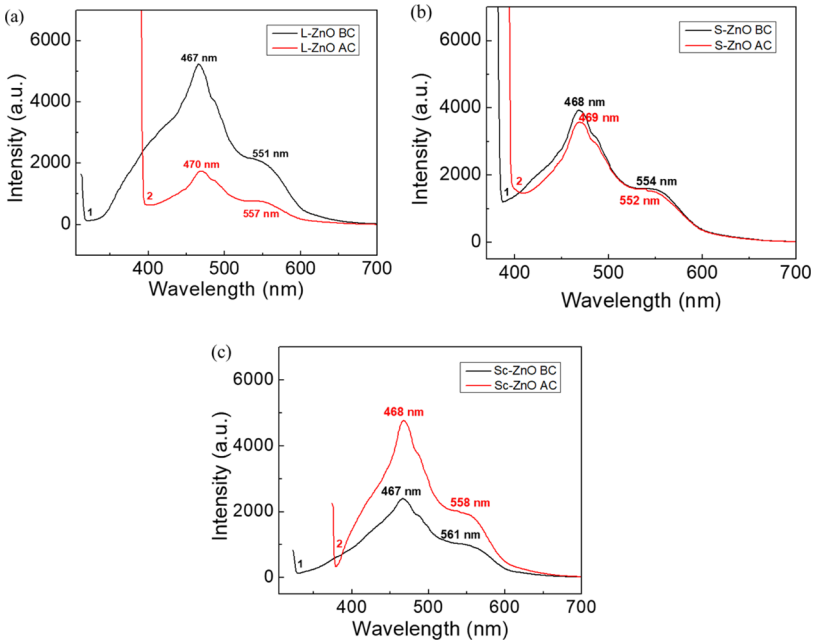

Figure 2. PL spectra of L-ZnO (a), S-ZnO (b) and Sc-ZnO (c) before (line 1) and after calcination (line 2)

emission peaks; one within the range 393−470 nm corresponding to band gap excitonic emission, whereas the other between 520 and 560 nm depicting the presence of defects.[40,41]

Emission spectra of ZnO nanoparticles are present in the visible region which can be due to the electron−hole recombination at a deep level emission present in the band gap occurring due to intrinsic point defects and surface defects such as oxygen vacancies, zinc interstitials, and incorporation of hydroxyl groups which take place in the crystal lattice during crystal growth within the solution.[42] There have been reports where calcination has shown both increase and decrease in PL intensities.[43,44] The PL spectra of L-ZnO and S-ZnO nanoparticles showed decrease in intensities with increased calcination temperatures. This may be due to aggregation of nanoparticles as a result of specific sintering between the individual grains at a higher sintering temperature. The transfer of energy to adjacent grains may be quenched due to the grain boundaries and surface defects arising because of calcination.[45] Sc-ZnO nanoparticles showed increase in intensities with increased calcination temperatures. It can be speculated that the increase in the calcination temperature leads to photo-denaturation of charge carriers and recombination centers in ZnO nanoparticles, thereby leading to increased intensities.[46] A blue emission was observed within the range 450−560 nm and a green emission was observed within the range 540−564 nm before and after calcination. The blue emission peaks were caused by defective structures present in the ZnO crystal particles corresponding to the singly ionized oxygen vacancy. The green emission was observed because of oxygen transition vacancy and interstitial oxygen.[47] The asymmetric nature of the emission spectra may be because of the presence of native defects in ZnO. The incidence of these defects increases the luminescence characteristics in case of ZnO present in a nano scale. Different parameters of ZnO nanoparticles such as size, morphology, surface roughness, surface functionalization, and so forth, have been observed to control these defect emissions.[48] These differential luminescence characteristics can be further exploited in various bio-applications.

2.2.3. XRD Studies. The crystalline properties and crystallite particle size of the biosynthesized L-ZnO, S-ZnO, and Sc-ZnO nanoparticles were analyzed using XRD as represented in Figure 3. The diffraction pattern and the sharp peaks clearly

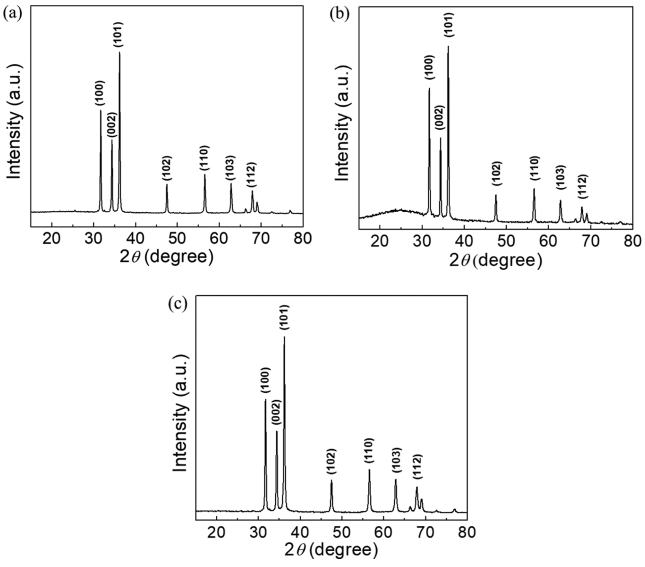

Figure 3. XRD spectra of biosynthesized L-ZnO (a), S-ZnO (b) and Sc-ZnO (c)

indicate the crystalline nature of the as-prepared ZnO nanoparticles. L-ZnO nanoparticles show presence of 2θ values such as 31.7, 34.38, 36.2, 47.5, 56.52, 62.82, and 67.9° (Figure 3a), S-ZnO nanoparticles show 2θ values such as 31.72, 34.38, 36.22, 47.52, 56.56, 62.86, and 67.92° (Figure 3b) whereas Sc-ZnO nanoparticles show 2θ values such as 31.72, 34.4, 36.22, 47.52, 56.56, 62.88, and 67.94° (Figure 3c).

It was observed that the significant 2θ values for biosynthesized ZnO nanoparticles coincide with standard 2θ

https://doi.org/10.1021/acsomega.1c05324
ACS Omega 2022, 7, 1914−1933

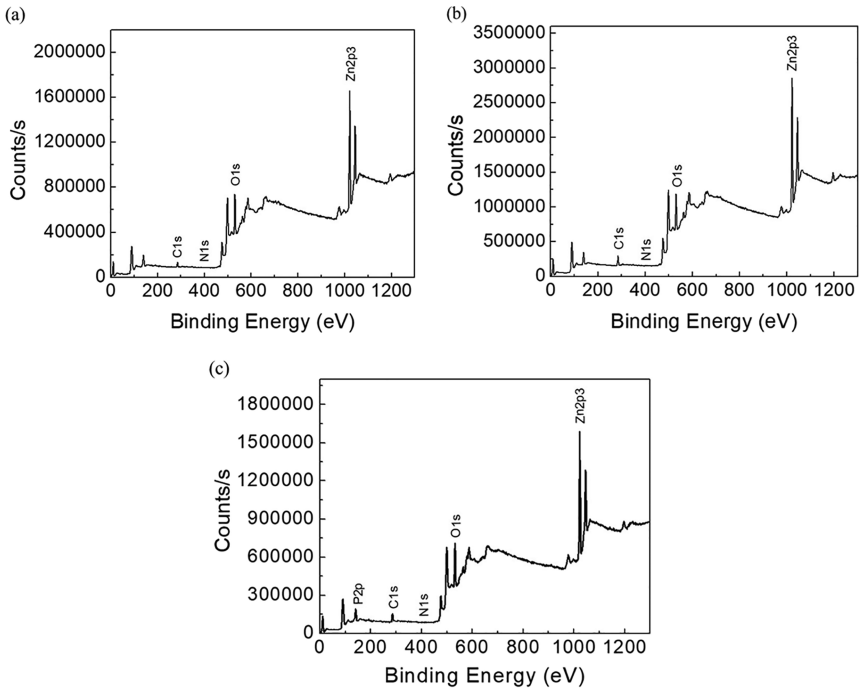

Figure 4. XPS spectra of biosynthesized L-ZnO (a), S-ZnO (b) and Sc-ZnO (c)

Table 1. XPS Results Showing the Elements with BE and Atomic % of the Synthesized L-ZnO, S-ZnO and Sc-ZnO Nanoparticles

sample	name	start BE	peak BE	end BE	FWMH eV	atomic %
L-ZnO	Zn $2p_3$	1028.5	1021.83	1013	4.46	32.5
	O 1s	540	531.1	526	4.11	48.75
	C 1s	298	285.61	279.5	4.33	18.1
	N 1s	408	395	394	0.58	0.65
S-ZnO	Zn $2p_3$	1028	1022.19	1013	4.17	29.34
	O 1s	538.5	531.25	524.5	4.26	39.92
	C 1s	293	285.17	278	4.48	30.27
	N 1s	408	401.02	394	1.88	0.47
Sc-ZnO	Zn $2p_3$	1028	1022.17	1013	4.34	23.24
	O 1s	537.5	531.34	526	4.39	38.57
	C 1s	294.5	285.22	277.5	4.39	17.71
	P 2p	144	139.92	126	4.49	20.14
	N 1s	408	400	394	0.71	0.33

values which are 31.770, 34.422, 36.253, 47.539, 56.603, 62.864, and 67.963° which have been indexed as (1, 0, 0), (0, 0, 2), (1, 0, 1), (1, 0, 2), (1, 1, 0), (1, 0, 3), and (1, 1, 2) planes. These values were found to coincide with that of a wurtzite structure of ZnO nanoparticles in its pure form (JCPDS no. 36-1415) upon comparison with XRD spectra of ZnO nanoparticles present in the already reported literature.[49] From the XRD spectra analysis, it is evident that the peak corresponding to (1, 0, 1) plane shows a higher intensity as compared to the rest of the peaks, thus indicating its preferential growth pattern toward that plane for the crystal growth.[50] As there are no undesirable peaks present in the XRD spectra, it underlines the high purity of the so-synthesized L-ZnO, S-ZnO and Sc-ZnO nanoparticles.

The average crystallite size of ZnO nanoparticles was further calculated with the help of Debye−Scherrer's formula (eq 2) as follows

$$d = k\lambda/\beta \cos(\theta) \quad (2)$$

where d is the mean crystallite size, k is the dimensionless shape factor, λ is the wavelength of Cu K_α X-ray radiation (1.54 Å), θ is the Bragg diffraction angle, and β is the full width at half-maximum of the diffraction peaks in the XRD spectra. Based upon the Debye−Scherrer formula, the average crystallite size for L-ZnO, S-ZnO, and Sc-ZnO was observed to be 37.25, 37.38, and 28.65 nm, respectively. Several previous studies have reported an average crystallite size within the range 23−61 nm based upon different reaction parameters influencing the physicochemical properties of ZnO nanoparticles.[51,52] There are previous reports showing the size estimates from TEM and XRD with remarkable difference.[53] The present study has reported the crystallite size calculated from XRD spectra with remarkable difference as compared to particle size from TEM micrographs. This may be because nanoparticles are composed of one or more crystallites. The crystallite size is assumed to be the size of a coherently diffracting domain, and it is not necessarily the same as the particle size because of which particle size calculated using

https://doi.org/10.1021/acsomega.1c05324
ACS Omega 2022, 7, 1914−1933

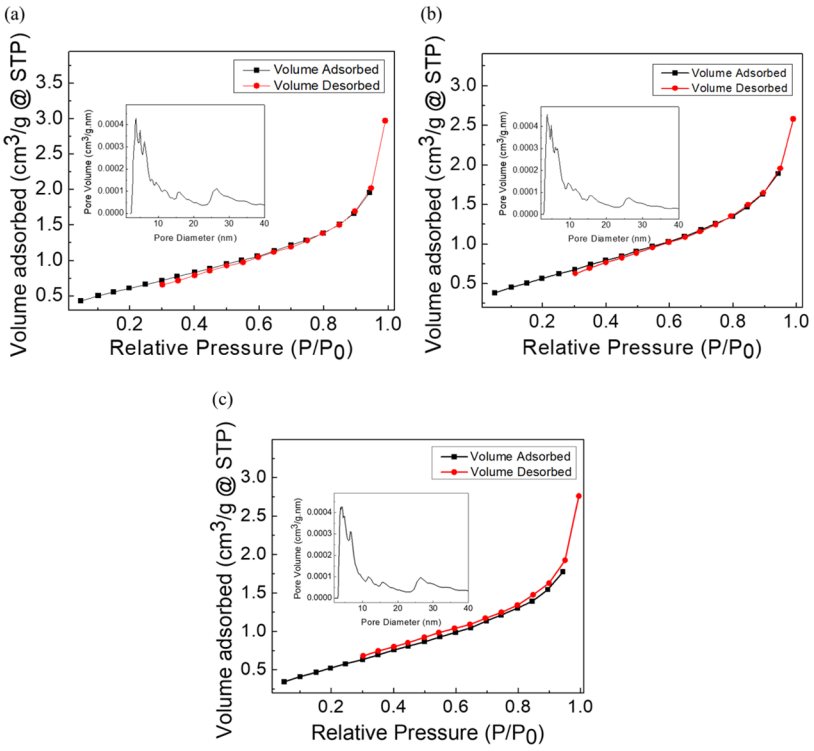

Figure 5. BET adsorption−desorption spectra and BJH pore size analysis (inset) of L-ZnO (a), S-ZnO (b) and Sc-ZnO (c) nanoparticles

TEM micrographs is always higher than the crystallite size estimated using XRD data.[54] Moreover, multiple nanocrsytallites determined by XRD spectra overlap to form a particle estimated by TEM images which explains higher values of particle sizes as compared to crystallite size.[55]

2.2.4. X-ray Photoelectron Spectroscopic Analysis. The elemental composition and the purity of L-ZnO, S-ZnO, and Sc-ZnO nanoparticles were characterized by the XPS analysis. From the XPS survey spectrum, it was found that the L-ZnO, S-ZnO and Sc-ZnO mainly consist of Zn and O while having a trace of C, N, and P (Figure 4a−c).

XPS results are shown in Table 1. Atomic % of Zn $2p_3$ and O 1s were the highest and represented the formation of ZnO. Low atomic % of impurities, such as Cls, N1s, P2p, and so forth were also observed which could attributed to impurities or biomolecules associated during ZnO biosynthesis.[56,57] C 1s at ∼285 eV was used as the binding energy (BE) reference; and therefore, it could be attributed to adventitious hydrocarbon.[50] The highest atomic % at BE peaks at 1022 eV corresponding to Zn $2p_3$ confirmed the presence of ZnO. O 1s at 531 eV, could be assigned to loosely bound oxygen (O_2^- ions) on the surface or oxygen deficient region within ZnO matrix which is similar to the previously reported studies.[58,59] The high-resolution XPS spectrum of O 1s at 531 eV is characteristic to the Zn−O and the OH group may have originated from the breaking of Zn−O−Zn bond and the formation of a Zn−OH bond, during the high-temperature synthesis under the ambient conditions.[55] Therefore, from the XRD and XPS analyses, it could be inferred that the as-synthesized ZnO was highly pure.

2.2.5. BET−BJH Surface Area and Pore Size Analysis. L-ZnO, S-ZnO, and Sc-ZnO nanoparticles were further characterized by the nitrogen gas adsorption−desorption analysis for obtaining the specific surface area, pore diameter, and the pore volume as represented in Figure 5a−c. BET specific surface area along with porosity parameters have been represented in Table 2. The BET specific surface area of the L-ZnO, S-ZnO, and Sc-ZnO was measured to be about 2.301, 2.187, and 2.107 m^2/g, respectively; whereas, conventional zinc oxide shows a specific surface area of 1.5 m^2/g.[60] L-ZnO, S-ZnO, and Sc-ZnO showed presence of specific surface areas in decreasing order. Previous reports showed a BET specific surface area within the range of 8−22 m^2/g.[52] The lower specific surface area may also be due to aggregation of nanoparticles which is evident from SEM images as well.[61] The average BJH pore diameter was ∼3−3.5 nm which demonstrates that the ZnO nanoparticles comprise of micro- and mesopores as per IUPAC definition. The BJH pore size distribution of all the ZnO nanoparticles (inset of Figure 5) shows major existence of pores within 5 nm. However, there are larger pores as well which coexist with the smaller pores.[62]

Table 2. Surface Area Analysis of Synthesized L-ZnO, S-ZnO and Sc-ZnO Nanoparticles

sample	name	results
L-ZnO	surface area	2.301 m^2/g
	pore volume	0.00402082 cm^3/g
	pore diameter	3.4129 nm
S-ZnO	surface area	2.187 m^2/g
	pore volume	0.00344201 cm^3/g
	pore diameter	3.41566 nm
Sc-ZnO	surface area	2.107 m^2/g
	pore volume	0.00375223 cm^3/g
	pore diameter	3.06614 nm

2.2.6. Morphological Analysis. Morphologies of L-ZnO, S-ZnO, and Sc-ZnO nanoparticles were analyzed with the help of FESEM analysis at different magnifications as represented in Figure 6. Nanocrystallites of spherical morphologies have been

https://doi.org/10.1021/acsomega.1c05324
ACS Omega 2022, 7, 1914−1933

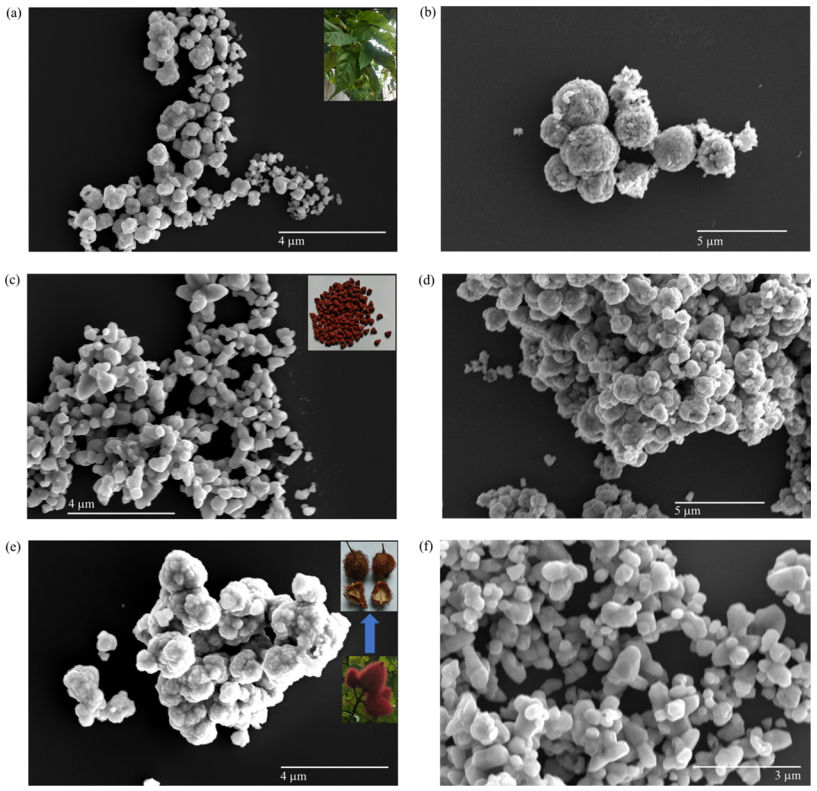

Figure 6. Morphological analysis of L-ZnO (a,b) with inset showing *B. orellana* leaf, S-ZnO (c,d) with inset showing *B. orellana* seed and Sc-ZnO (e,f) with inset showing *B. orellana* seed coat at different FESEM magnifications.

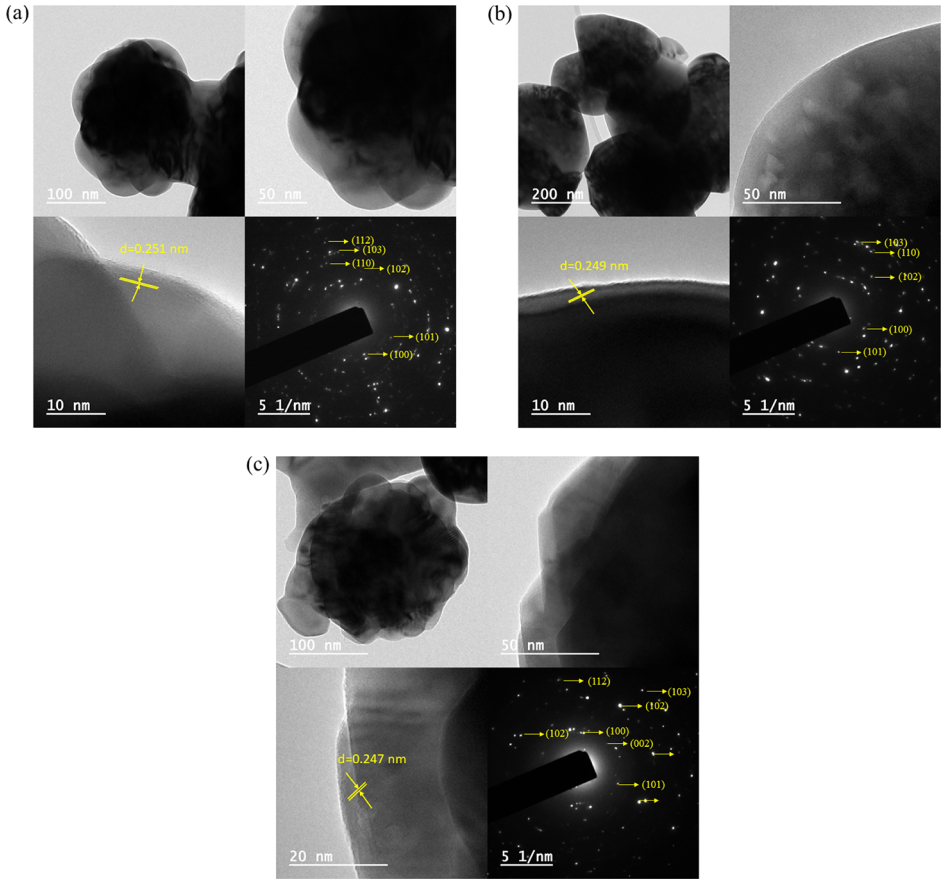

Figure 7. TEM images, lattice fringes and SAED patterns of L-ZnO (a), S-ZnO (b) and Sc-ZnO (c) nanoparticles.

https://doi.org/10.1021/acsomega.1c05324
ACS Omega 2022, 7, 1914−1933

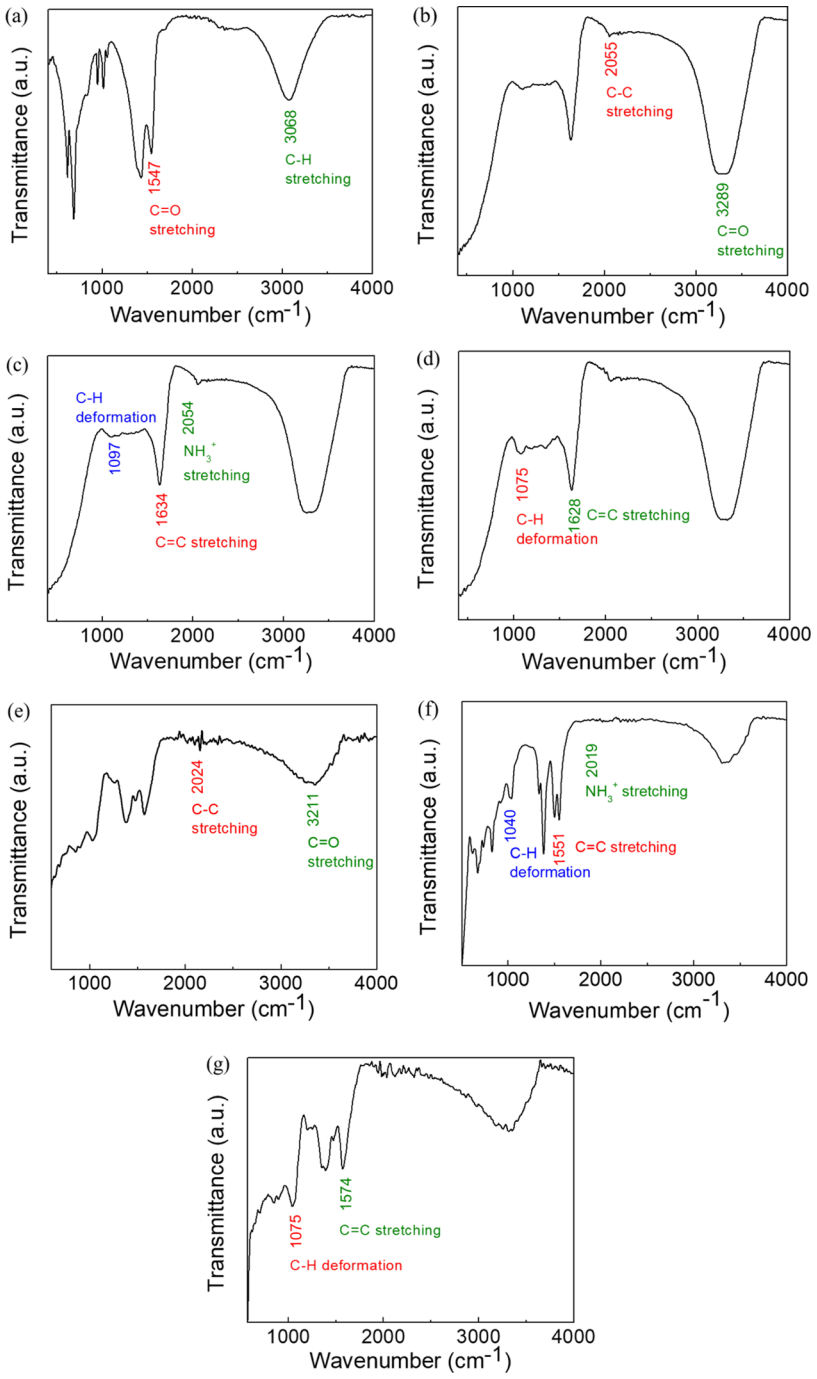

Figure 8. ATR-IR spectra of zinc acetate (a), BL extract (b), BS extract (c), BSc extract (d), L-ZnO (e), S-ZnO (f) antd Sc-ZnO (g)

observed in case of L-ZnO at lower magnification as represented in Figure 6a and at higher magnification as represented in Figure 6b. Nanocrystallites of spherical shapes have been observed within the size range 114−344 nm. Inset of Figure 6a shows *B. orellana* leaf. These nanocrystallites aggregate to form larger nanospheres ranging from 343 to 571 nm. Nanocrystallites of spherical and rod-like morphologies have been observed in case of S-ZnO at higher magnification as represented in Figure 6c and at lower magnification as represented in Figure 6d. Nanocrystallite spheres and rods have been observed within the size range 220−440 and 330−660 nm, respectively. Inset of Figure 6c shows *B. orellana* seed. These nanocrystallites aggregate to form larger nanoflowers ranging from 344 nm to 1.552 μm. Nanocrystallites of spherical and rod-like morphologies have been observed in case of Sc-ZnO at lower magnification as represented in Figure 6e and at higher magnification as represented in Figure 6f. Nanocrystallite spheres and rods have been observed within the size range 257−428 and 428−857 nm, respectively. Inset of Figure 6e shows *B. orellana* seed coats. These nanocrystallites aggregate to form larger nanoflowers ranging from 588 nm to 1.764 μm. It is evident from these results that all the particles are homogenously distributed which is critical for their bio-activities. There are several studies showing ZnO nanoparticles within the size range 110−660 nm depending upon different synthesis methods which in turn influence their

https://doi.org/10.1021/acsomega.1c05324
ACS Omega 2022, 7, 1914−1933

physicochemical parameters.[63,64] The increase in the particle size as compared to individual nano-crystallites is due to overlapping and aggregation of nanoparticles over one another. EDS was conducted to estimate the purity of L-ZnO, S-ZnO, and Sc-ZnO nanoparticles (Figure S1). EDS analysis of these ZnO nanoparticles was performed in auto mode to depict overall elemental composition and specifically for zinc (Zn) and oxygen (O) to analyze their weight percentage. The elements Zn and O have been observed to contribute majority percentage in all three ZnO nanoparticles. The impurities such as carbon (C), aluminium (Al) and silicon (Si) were observed in trace quantities. The presence of these impurities can be justified as the samples were loaded on silicon vapor which was placed on aluminium stub during EDS analysis and carbon tape was used for keeping the sample in place. The weight percentages of Zn and O were observed to be 81.48 and 18.52 for L-ZnO (Figure S1a) and Sc-ZnO (Figure S1c), whereas 72.31 and 27.69 for S-ZnO (Figure S1b) which is close to the expected stoichiometric mass percent (80.3 for Zn and 19.7 for O) which was in accordance with previous reports.[26,65]

Morphological characteristics and particle sizes of L-ZnO, S-ZnO, and Sc-ZnO were further confirmed using TEM micrographs at different magnifications as represented in Figure 7. L-ZnO shows the presence of spherical particles within the size range 169−259 nm (Figure 7a), S-ZnO shows the presence of almond-like morphologies within the size range 304−465 nm (Figure 7b), whereas Sc-ZnO shows the presence of spherical particles within the size range 278−654 nm (Figure 7c). Previous studies show ZnO nanoparticles within the size range 100−650 nm depending upon different synthesis methods which in turn influence their physicochemical parameters.[66,67]

The TEM images revealed that the ZnO nanoparticles are predominantly spherical in shape in L-ZnO and Sc-ZnO; whereas, almond-like shapes in case of S-ZnO. L-ZnO, S-ZnO, and Sc-ZnO have been observed to show crystalline planes having an interplanar *d*-spacing of 0.251, 0.249, and 0.247 nm, respectively, all of which corresponds to the (1, 0, 1) plane, whereas previously reported studies show the predominant presence of (1, 0, 1) plane.[68] The SAED patterns of L-ZnO, S-ZnO, and Sc-ZnO predominantly display concentric rings having bright spots corresponding to (1, 0, 0), (0, 0, 2), (1, 0, 1), (1, 0, 2), (1, 1, 0), (1, 0, 3), and (1, 1, 2) planes. Similar results have been observed in the XRD analysis as well. Thus, these ZnO nanoparticles were confirmed for a highly crystalline and monodisperse nature which was in congruence with the previous studies.[69,70]

2.2.7. ATR-IR Spectra Analysis. ATR-IR analysis of the ZnO nanoparticles, *B. orellana* leaf, seed, and seed coat extracts and zinc precursor salts was performed for determining the associated molecules playing a role in biosynthesis of ZnO nanoparticles. ATR-IR spectra of zinc acetate salt (a), BL extract (b), BS extract (c), BSc extract (d), L-ZnO (e), S-ZnO (f), and Sc-ZnO (g) have been depicted in Figure 8. ATR-IR spectra of zinc acetate which has been used as a zinc precursor salt represent notable peaks at 3068.65 and 1547.12 cm^{-1} which coincide with peaks of ZnO nanoparticles (Figure 8a). ATR-IR spectra of BL extract exhibit distinguished peaks at 3289.21 and 2055.26 cm^{-1} (Figure 8b). ATR-IR spectra of BS extract exhibit distinguished peaks at 2054.20, 1634.23 and 1097.07 cm^{-1} (Figure 8c). ATR-IR spectra of the BSc extract exhibit distinguished peaks at 1628.61 and 1075.53 cm^{-1} (Figure 8d). ATR-IR spectra of L-ZnO nanoparticles exhibit noticeable peaks at 3211.40 and 2024.40 cm^{-1} (Figure 8e). ATR-IR spectra of S-ZnO nanoparticles exhibit noticeable peaks at 2019.55, 1551.87 and 1040.63 cm^{-1} (Figure 8f). ATR-IR spectra of Sc-ZnO nanoparticles exhibit noticeable peaks at 1574.05 and 1042.44 cm^{-1} (Figure 8g).

The peaks at 3289.21 and 3211.40 cm^{-1} represent O−H stretching, $-CONH_2$ stretching, N−H stretching along with C═O stretching. The peaks at 2055.26, 2054.20, 2024.40, and 2019.55 cm^{-1} signify C−C stretching and $-NH_3^+$ stretching in amino acids. The peaks at 1634.23, 1628.61, 1574.05, and 1551.87 cm^{-1} denote C═C stretching, C═O stretching, and N−H deformation. The peaks at 1097.07, 1075.53, 1042.44, and 1040.63 cm^{-1} indicate C−H deformation, C−O stretching in esters, and ethers together with C−N stretching in amines. The decrease in wavenumbers of corresponding functional groups in L-ZnO, S-ZnO, and Sc-ZnO nanoparticles as compared to the BL, BS and BSc extracts denote their association with respective ZnO nanoparticles.[71,72] To summarize, ATR-IR spectra showed that the functional groups such as hydroxyl, amino, carboxylic groups present in different phytochemicals from BL, BS, and BSc extracts are involved in the reduction and stabilization of L-ZnO, S-ZnO, and Sc-ZnO. Previous reports have shown that proteins and carbohydrates involving C═O stretching, $-NH_3^+$ stretching and O−H stretching are responsible for stabilizing ZnO nanoparticles.[17,73,74]

2.2.8. GC−MS Analysis. BL, BS, and BSc extracts were analyzed for identification of probable molecules with the help of GC−MS analysis as represented in Figure S2. It has been observed that BL extract indicates existence of aromatics and vinyl compounds (Figure S2a), BS extract indicates existence of phenolics, flavonoids, aromatics and fatty acids (Figure S2b) and BSc extract indicates existence of phenolics, steroids, flavonoids, carotenoids, fatty acids and long chain hydrocarbons (Figure S2c).

2.2.9. HR-MS Analysis. BL, BS and BSc aqueous extracts were analyzed for identification of probable molecules with the help of HR-MS based upon their m/z ratios as represented in Figure S3. BL extract confirmed the presence of molecular fragments with m/z ratios 139 and 192 corresponding to beta-copaene and alloaromadendrene, respectively (Figure S3a).[75,76] The BS extract confirmed the presence of molecular fragments with m/z ratios 273 and 717 corresponding to geranylgeraniol and andrographolide, respectively (Figure S3b).[77,78] The BSc extract confirmed the presence of molecular fragments with m/z ratios 219, 284 and 315 corresponding to octadecenal, vaccenic acid and isocarpesterol, respectively (Figure S3c).[79−81] These biomolecules were also seen in GC−MS analysis thus underlining the role of flavonoids, steroids, phenolics and aromatic compounds in the biosynthesis of ZnO nanoparticles.[82]

2.2.10. NMR Analysis. BL, BS, and BSc extracts were analyzed for identification of probable molecules with the help of ^1H NMR using D_2O as solvent which has been represented in Figure S4a−c. Chemical shifts were observed in the characteristic range of alcohols (3.5−5.5 ppm), primary alkyl groups (∼0.7−1.3 ppm), secondary alkyl groups (∼1.2−1.6 ppm), phenolic hydroxyl groups (4−7 ppm), and aromatic protons of C-ring of flavonoids (∼4.2 ppm).[83,84] Strong peak of D_2O was observed at 4.8 ppm. Thus, BL, BS, and BSc extracts showed presence of aromatics, flavonoids, steroids, alcohols, phenolics, and alkyl groups.

https://doi.org/10.1021/acsomega.1c05324
ACS Omega 2022, 7, 1914−1933

2.3. Plausible Mechanism of Synthesis of ZnO Nanoparticles. The plausible mechanism with which ZnO nanoparticles are synthesized using BL, BS and BSc extracts has been represented in Figure 9. Zinc acetate which acts as the zinc precursor salt dissociates in aqueous environment to form Zn^{2+} and acetate ions. Various phytochemicals such as aromatics, flavonoids, steroids and phenolics present in the plant extract stabilizes the Zn^{2+} ions by chelating it thereby forming a complex. Flavonoids, steroids, and phenolics with excess hydroxyl groups play a major role during the synthesis process of ZnO nanoparticles.[85] Beta-copaene present in BL extract is an aromatic compound (Figure 9a), andrographolide present in BS extract is a flavonoid molecule (Figure 9b) and isocarpesterol present in BSc extract is a steroid molecule (Figure 9c) which associates with the zinc precursor thereby directing the biosynthesis of ZnO nanoparticles. The freely available Zn^{2+} ions associate with the active sites which readily chelate the freely available ions by virtue of their potential to donate electrons via weak hydrogen bonding thereby forming a stable complex. In this process, the Zn^{2+} ions reduce to form metallic Zn atoms. However, the metallic Zn atoms take up atmospheric oxygen thereby forming ZnO nanoparticles due to the superactive nature of Zn^{0} entities. Further decomposition of this complex results the liberation of water molecules thus forming ZnO nanoparticles coated with biomolecules from the respective extracts.[86] The association of biomolecules with the ZnO nanoparticles has been confirmed by ATR-IR, GC−MS, HR-MS, and NMR analysis. The so-formed ZnO nanoparticles are highly stable and its association with different biomolecules present in these extracts further enhance the stability of these nanoparticles. These biomolecules also act as binding entities thus directing shape and size of the biosynthesized ZnO nanoparticles due to which different physicochemical properties are seen in ZnO nanoparticles in spite of using the same precursor salt.

2.4. Anti-bacterial Activity of ZnO Nanoparticles. As ZnO is known for its antibacterial properties, its *in vitro* antibacterial potential has been evaluated using various bacterial species like *E. coli*, *S. aureus*, *P. aeruginosa*, *B. subtilis*, and so forth.[87,88] In this study, the antibacterial properties of ZnO nanoparticles synthesized using *B. orellana* leaf, seed, and seed coat extracts were analyzed before and after calcination with the help of Gram positive (*S. aureus*, *B. subtilis*) together with Gram negative (*E. coli*, *P. aeruginosa*) microorganisms using a well-based diffusion technique as represented in Figure 10a−f. L-ZnO, S-ZnO, and Sc-ZnO were tested for antibacterial activity at different concentrations ranging from 0.625 to 10 mg/mL before and after calcination in triplicates. BL, BS, and BSc extracts were also tested against these microorganisms which did not show any antibacterial activity against any of these micro-organisms.

L-ZnO was observed to exhibit antibacterial activity only against *S. aureus* and *B. subtilis*, S-ZnO showed antibacterial activity only against *E. coli* whereas Sc-ZnO showed antibacterial activity only against *S. aureus* before calcination. However, all the L-ZnO, S-ZnO and Sc-ZnO nanoparticles exhibited lack of antibacterial properties against any of these micro-organisms after calcination. Zones of inhibition of uncalcinated L-ZnO, S-ZnO and Sc-ZnO at different concentrations have been represented in Table 3. Thus, L-ZnO, S-ZnO, and Sc-ZnO show antibacterial potential in decreasing order. While there are extensive studies which show excellent antibacterial activities of ZnO nanoparticles,[89,90] this

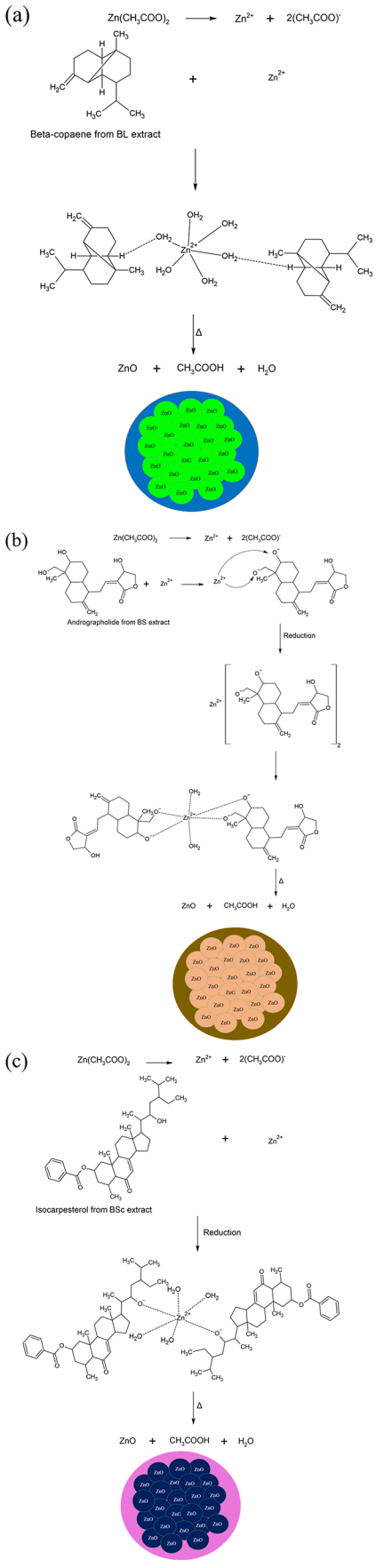

Figure 9. Plausible mechanism of ZnO biosynthesis using BL (a), BS (b) and BSc (c) extracts

https://doi.org/10.1021/acsomega.1c05324
ACS Omega 2022, 7, 1914−1933

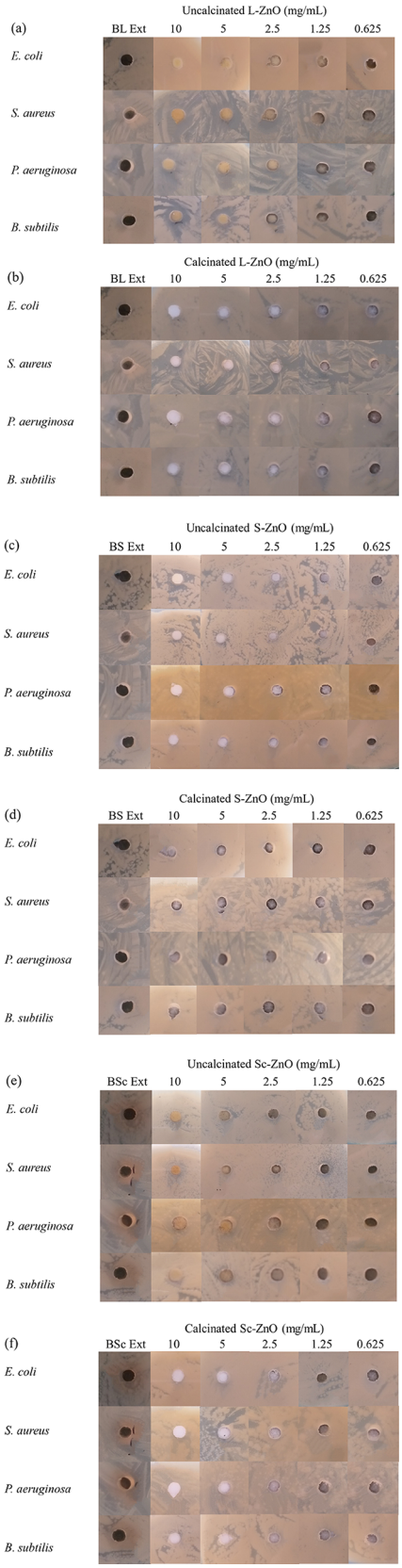

Figure 10. Antibacterial activity of uncalcinated and calcined L-ZnO (a,b), S-ZnO (c,d) and Sc-ZnO (e,f) nanoparticles before and after calcination at different concentrations against Gram positive (*S. aureus*, *B. subtilis*) together with Gram negative (*E. coli*, *P. aeruginosa*) micro-organisms.

is the first report where weak or no antibacterial activity has been reported to the best of our knowledge.

There are several reports elaborating antimicrobial properties of ZnO nanoparticles against various microorganisms. Even though exact underlying mode of action responsible for antibacterial properties of ZnO nanoparticles is still not completely understood, there are several studies which have shown antibacterial properties of ZnO nanoparticles against Gram positive and Gram negative bacteria. The antibacterial properties of ZnO nanoparticles can be majorly attributed to the disruption of cell membrane, generation of ROS and Zn^{2+} release. Electrostatic interactions of ZnO nanoparticles with the bacterial cell membrane facilitate their association. A physical contact between the nanoparticles and bacterial cells results in aberrations on the cell membrane which results in membrane leakage. Zn^{2+} release affects bacterial growth by inhibiting active transport, hampering metabolism of amino acids and inactivating various enzymes within the cell. In addition to this, increased ROS production hamper the vital cellular functioning thus resulting in cell death. All these mechanisms collectively result in cell death, thereby contributing to the antibacterial properties of ZnO nanoparticles.[91,92] However, different factors such as particle size, morphology, illumination conditions, concentration, surface functionalization, surface defects, and so forth, have been reported to affect the toxicity potential of ZnO nanoparticles.[12] Size and concentration dependent toxicity have been observed in Gram-positive and Gram-negative microorganisms. Antibacterial potential was inversely proportional to particles size. The reason behind this is larger surface area of smaller nanoparticles leads to higher ROS generation which ultimately enhances its antibacterial potential.[10,93] Similar results have been obtained in the present study. L-ZnO nanoparticles are of smallest size and show highest antibacterial activity. There are various particles above 200 nm in case of S-ZnO and Sc-ZnO because of which it may show restricted cellular penetration thereby affecting its antibacterial potential.[94]

Surface functionalization of ZnO nanoparticles have also been observed to influence its antibacterial potential. Even though surface modification has been known to impart stability and prevent aggregation of ZnO nanoparticles, it also influences release of Zn^{2+} ions and ROS generation which in turn affects their antibacterial potential.[95] As L-ZnO, S-ZnO, and Sc-ZnO are biosynthesized using BL, BS, and BSc extracts, they are functionalized with different biomolecules which justifies their differential antibacterial potential. The BL extract indicates existence of aromatics and vinyl compounds; the BS extract indicates existence of phenolics, flavonoids, aromatics, and fatty acids; and the BSc extract indicates existence of phenolics, steroids, flavonoids, carotenoids, fatty acids, and long chain hydrocarbons. Aromatic compounds, flavonoids, and fatty acids can easily penetrate through the lipid bilayer and cause damage to the bacterial cell by ultimately killing it. However, steroids and phenolics being bulkier molecules cannot transverse the lipid bilayer without any transporters. Hence, L-ZnO shows higher antibacterial activity as compared to S-ZnO and Sc-ZnO. Also, the surface coating with biomolecules from BS and BSc extracts has been observed to impart inertness to the nanoparticles thereby translating into their biocompatible nature. This has been already observed previously in case of gold and silver nanoparticles synthesized using the *Albizia lebbeck* flower extract.[96,97] The presence of an inert coating around ZnO nanoparticles affects the release of

https://doi.org/10.1021/acsomega.1c05324
ACS Omega 2022, 7, 1914−1933

Table 3. Antibacterial Activity of Uncalcinated L-ZnO, S-ZnO and Sc-ZnO against Different Micro-organisms

		concentration of ZnO nanoparticles (mg/mL)				
nanoparticles	micro-organisms	10	5	2.5	1.25	0.625
L-ZnO	*E. coli*					
	S. aureus	19 mm	11 mm	9 mm		
	P. aeruginosa					
	B. subtilis	14 mm	10 mm			
S-ZnO	*E. coli*	8 mm				
	S. aureus					
	P. aeruginosa					
	B. subtilis					
Sc-ZnO	*E. coli*					
	S. aureus	10 mm				
	P. aeruginosa					
	B. subtilis					

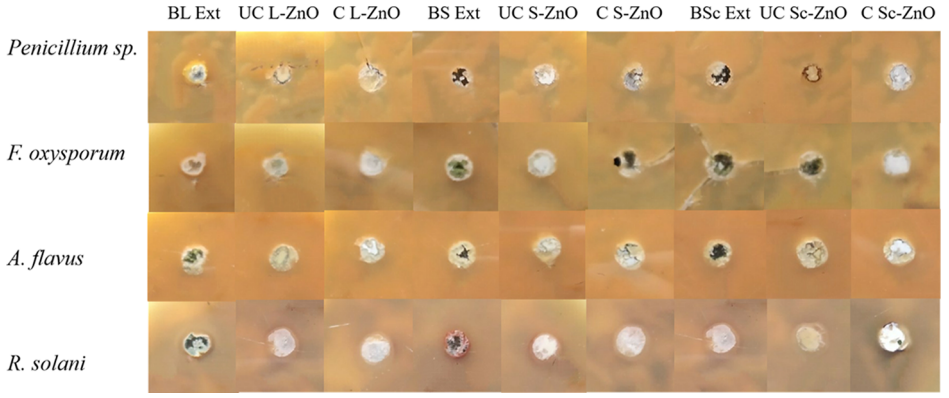

Figure 11. Antifungal activity of uncalcinated and calcined L-ZnO, S-ZnO and Sc-ZnO nanoparticles before and after calcination at a concentration of 10 mg/mL against different fungi (*Penicillium* spp., *F. oxysporum*, *A. flavus*, *R. solani*)

Zn^{2+} ions into the environment, which in turns decreases the damage to the bacterial cell upon interaction with ZnO nanoparticles ultimately hampering its antibacterial potential.[98] Uncalcinated ZnO nanoparticles have shown a higher antibacterial activity in comparison with calcined ones. This has been observed in case of L-ZnO, S-ZnO, and Sc-ZnO. Calcination carried out at higher temperatures adversely affects the antibacterial potential of ZnO nanoparticles by causing aggregation of nanoparticles which in turn leads to increase in size.[99] Penetration of larger nanoparticles into the bacterial cell becomes difficult. Also, larger nanoparticles imply decreased surface area which affects ROS generation and Zn^{2+} release.[10] Decreased antibacterial activity upon calcination is a cumulative effect of all these factors.

Selective toxicity of ZnO nanoparticles against different microorganisms can be due to differences in the membrane structure as nanoparticles are known to first interact with the cell wall before entering the bacterial cell. Gram negative bacteria have been observed to show higher susceptibility to the action of ZnO nanoparticles in comparison with Gram positive bacteria. Different parameters such as cell membrane structures, physiological and metabolic state of the bacteria and extent of interaction between the nanoparticles and the bacteria are responsible for its selective toxicity.[100] The cellular wall present in Gram positive bacteria is made up of an approximately 20 nm thick peptidoglycan layer which constitutes linear polysaccharides cross-linked to one another. However, the peptidoglycan layer of Gram negative bacteria is only 7−8 nm thick. However, it also contains a lipopolysaccharide layer above it. The presence of a thick lipopolysaccharide layer in Gram negative microorganisms results in an increased resistance against nanoparticles in comparison with Gram positive microorganisms. In some cases, the presence of peptidoglycan layers restricts entry of ZnO nanoparticles in Gram positive bacteria, thus showing higher antibacterial potential against Gram negative bacteria. This selective nature for entry of ZnO nanoparticles into the micro-organisms largely depends upon the physicochemical properties of the nanoparticles.[101] Here, we have observed selective toxicity in Gram positive bacteria whereas Gram negative bacteria showed no antibacterial activity when treated with L-ZnO and Sc-ZnO. Sc-ZnO showed antibacterial activity only against *S. aureus* and not *B. subtilis*. The reason for this might be the potential of *B. subtilis* to produce exopolysaccharides. The presence of exopolysaccharides acts as a barrier for penetration of nanoparticles into the bacterial cell.[102] These exopolysaccharides entrap the nanoparticles before entering the bacterial cell thereby protecting the bacteria from detrimental effects of nanoparticles. It is due to the presence of these exopolysaccharides in *B. subtilis* that it fails to show any antibacterial activity. On the contrary, S-ZnO showed selective toxicity against Gram negative and not Gram positive microorganisms. In case of S-ZnO, the antibacterial activity was observed only against *E. coli* and not *P. aeruginosa*. This is because *P. aeruginosa* upregulates production of extracellular flagellin which causes agglomeration of nanoparticles thereby avoiding direct contact with the bacterial cell. It also produces the pigment pyocyanin which is capable of inactivating metal

https://doi.org/10.1021/acsomega.1c05324
ACS Omega 2022, 7, 1914−1933

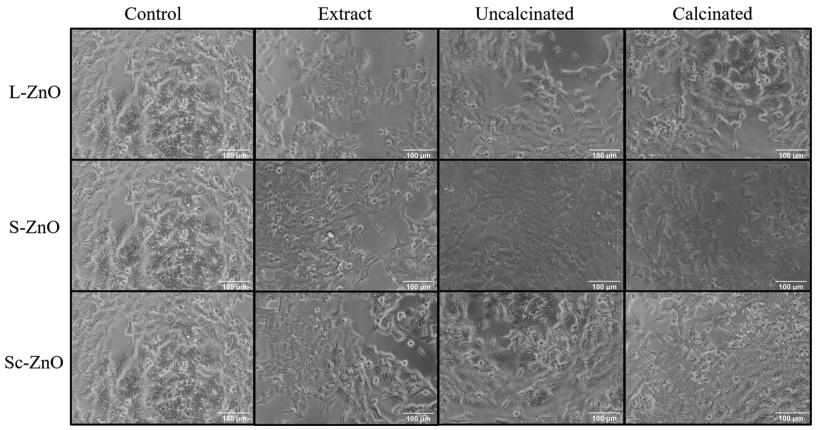

Figure 12. Cytotoxicity studies of uncalcinated and calcined L-ZnO, S-ZnO and Sc-ZnO nanoparticles before and after calcination at a concentration of 100 μg/mL against HCT-116 cancer cells

ions released by nanoparticles thereby neutralizing its toxic effect.[103]

Also, exposure to sub-lethal doses of ZnO nanoparticles can result in development of defense mechanisms thereby developing tolerance against ZnO nanoparticles. This process is known as hormesis which functions at two different levels for developing resistance. One of these mechanisms shows enzyme-level involvement whereas the other mechanism involves transcription and genome-based sub-levels. At enzymatic and transcriptional levels, antioxidant enzymes get activated upon sensing increased ROS levels which reverse their effect thereby neutralizing their lethality. At the genome level, increased ROS can result in DNA damage which in turn activate different repair mechanisms. Under unprecedented circumstances, the error-prone DNA polymerase might add abnormal bases during the repair process thereby imparting genomic plasticity which results in resistance against metal-based nanoparticles.[104] Thus, all these factors cumulatively contribute to the selective lethality of ZnO nanoparticles against various micro-organisms.

2.5. Anti-fungal Activity of ZnO Nanoparticles. As ZnO is known for its antifungal properties, its *in vitro* antifungal potential has been evaluated using various fungal species such as *Penicillium expansum*, *Fusarium solani*, *Colletotrichum gloeosporioids*, *Aspergillus flavus*, *Rhizoctonia solani*, *Candida albicans*, and so forth.[91,105,106] In this study, the antifungal properties of ZnO nanoparticles synthesized using *B. orellana* leaf, seed, and seed coat extracts were analyzed before and after calcination with the help of different fungi (*Penicillium* sp., *F. oxysporum*, *A. flavus*, *R. solani*) using well-based diffusion technique as represented in Figure 11. The biosynthesized ZnO nanoparticles were tested for antifungal activity at a concentration of 10 mg/mL before and after calcination in triplicates. The BL, BS, and BSc extracts were also tested against these fungi which did not show any antifungal activity against any of these fungi. These ZnO nanoparticles showed no antifungal activity against all four fungi before and after calcination. While there are extensive studies which show excellent antifungal activities of ZnO nanoparticles,[107] this is the first report where no antifungal activity has been reported to the best of our knowledge.

As compared to the tremendous amount of work focusing on antibacterial properties of ZnO nanoparticles, fewer studies have been conducted for understanding their antifungal potential and factors affecting the same. ZnO nanoparticles conventionally do show antifungal properties by depending upon one or more mechanisms including disruption of vital cell structures like cell wall, cell membrane, cell organelles, and so forth, arrest of important biological pathways associated with related biomacromolecules, loss of control over anti-oxidant system via ROS generation and/or release of Zn^{2+} ions.[108] However, there is very little understanding about the molecular mechanisms involved in antifungal properties of ZnO nanoparticles as the relevant research is still in its infancy. Based upon the limited information available, different parameters available affecting the antifungal efficiency of ZnO nanoparticles include size, shape, solubility, structure, concentration, surface functionalization, surface activity, and so forth.[109] Solubilities of ZnO nanoparticles have been observed to significantly affect its antifungal properties.[110] In the present study, ZnO nanoparticles have been observed to form a dispersion in water which would result in lower proportion of Zn^{2+} release adversely affecting its antifungal properties. Even though the surface functionalization has been known to make ZnO nanoparticles stable, biocompatible, functional, sensitive, and selective in action along with improving their antifungal potential, direct molecular interaction with these biomolecules can result in strong association thus imparting inertness to these nanoparticles as a result of which antifungal potential would be adversely affected.[111] Similar results have been observed in the present study where strong association with these nanoparticles might have affected Zn^{2+} release and ROS generation ultimately leading to non-antifungal nature.

Apart from physicochemical characteristics of ZnO nanoparticles, the fungal membrane structure shows a remarkable influence upon their antifungal activity. The fungal cell wall is made up of β-1,3-D-glucan, β-1,6-D-glucan macroproteins, other glucans, mannans, chitin, proteins, polysaccharides, and lipids which impart rigidity to the structure.[112] This rigid nature of the fungal cell wall makes it further difficult for the ZnO nanoparticles to penetrate inside the fungal cell and cause necessary damage crucial for antifungal potential. Different fungi might also develop resistance mechanisms such as modulation of stress responses to withstand sub-optimal concentration of ZnO nanoparticles. Upregulation of anti-oxidant enzymes such as glutathione reductase and superoxide dismutase has been observed in *Sclerotinia homoeocarpa*. Elevated expression levels of ShSOD2 and Shgst1 genes help the fungal cells in neutralizing elevated ROS levels caused due to ZnO nanoparticles thus helping in maintaining fungal cell

https://doi.org/10.1021/acsomega.1c05324
ACS Omega 2022, 7, 1914−1933

viability.[113] Similarly, modulation of ergosterol synthesis is also observed in fungal cells in response to exposure to elevated ROS levels. Modulation of unsaturation of phospholipids in the lipid bilayer also takes place in response to oxidative stress. These elevated ergosterol levels and increase in unsaturated phospholipids constituting the fungal cell wall thus increasing membrane fluidity inhibiting membrane damage thereby protecting fungal cells from action of ZnO nanoparticles.[114] Thus, all these factors cumulatively influence antifungal properties of ZnO nanoparticles.

2.6. Cytotoxicity Studies. Even though ZnO nanoparticles are known for its biocompatible nature, previous studies have reported both biocompatibility and anticancer activities against mammalian cells.[115,116] In this study, the cytotoxicity studies of ZnO nanoparticles synthesized using *B. orellana* leaf, seed, and seed coat extracts were analyzed before and after calcination against HCT-116 cancer cells using trypan blue staining as represented in Figure 12. Cytotoxicity studies were performed using these biosynthesized ZnO nanoparticles at a concentration of 100 μg/mL before and after calcination in triplicates. BL, BS, and BSc extracts were also tested against these cancer cells which did not show any cytotoxic activity against any of these cancer cells. L-ZnO, S-ZnO, and Sc-ZnO nanoparticles showed no cytotoxicity against these cancer cells before and after calcination thus underlining their biocompatible nature.

There are reports showing anticancer properties and biocompatible nature of ZnO nanoparticles.[117,118] Thus, the mechanism behind the cytotoxicity of ZnO nanoparticles is still ambiguous. Biocompatibility of ZnO nanoparticles has been observed to depend upon various physico-chemical characteristics. Before the entry of nanoparticles into medicinal framework as alternative antibacterial or dye degradable material, it is necessary to evaluate the biocompatibility of the synthesized nanoparticles.[119] The clinical trials on nanoparticles are still rare due to insufficient data on the biocompatibility and toxicity *in vitro*.

One of the mechanisms contributing to the toxicity of ZnO nanoparticles is release of Zn^{2+} ions by virtue of ZnO dissolution. Dissolved free-zinc from either ZnO nanoparticles or $ZnCl_2$ induces apoptosis or necrosis in endothelial and epithelial cells by damaging mitochondrial function followed by elevation of intracellular reactive-oxygen species.[120] Toxicity of ZnO nanoparticles is also influenced by surface functionalization of these nanoparticles. The interaction between the ZnO and phytochemical coating them influences the release of Zn^{2+} ions into the aqueous environment.[97] Strong association between the coating and ZnO nanoparticles affects the release of Zn^{2+} ions into the environment, which in turn decreases the damage to the cell upon interaction with ZnO nanoparticles ultimately hampering its cytotoxicity against cancer cells. Excess coating onto the ZnO nanoparticles reduces the release of Zn^{2+} ions, thereby reducing their bioavailability to interact and penetrate the cell thus contributing to its biocompatible nature.

Similarly, the dissolution of ZnO nanoparticles in an aqueous medium also determines its cytotoxicity against cancer cells. The extent of dissolution of ZnO nanoparticles determines the amount of Zn^{2+} ions released thus contributing to its cytotoxicity. The extent of Zn^{2+} ions dissociated from ZnO nanoparticles in the culture medium is difficult to calculate as it is governed by multiple parameters such as composition, surface functionalization, exposure time, temperature, and so forth.[121] ZnO nanoparticles coated with phytochemicals from plant extracts display a low solubility in the culture medium thus resulting in slow release of ions. Due to this slow release, Zn^{2+} ions are not available to interact with the cancer cells which in turn results in lack of penetration inside the cell and therefore will not be able to show toxicity against any mammalian cells even by using various growth media. Due to its biocompatible nature, these ZnO nanoparticles are suitable to be used as carrier molecules in drug delivery applications.

The use of nanoparticles as a carrier system for drug delivery applications raises concerns regarding their disposal within the host system. However, in case of ZnO nanoparticles, as zinc is among the important micronutrients actively assimilated in both plant and mammalian systems, it can be utilized for functioning of various biomacromolecules, enzymes and metalloproteins, thereby affecting catalytic and structural functions.[122]

Even though different plant parts from the same plant source, that is, *B orellana*, has been used in the biosynthesis of ZnO nanoparticles, it is evident that there is an observable difference in their physicochemical properties and bioactivities. Thus, biomolecules contributed by these extracts seem to be playing a significant role in modulating the properties of these nanoparticles. More research study on zinc oxide nanoparticles is needed to explore the role of different biomolecules in determining their physicochemical parameters and its influence on biomedical applications. Also, a comprehensive analysis of effect of various parameters such as size, morphology, surface potential, surface modification, retention time, bio-availability, and so forth, of ZnO nanoparticles on mammalian and plant host systems is essential for its successful use which would require further *in vivo* studies.

3. CONCLUSIONS

Thus, we have reported a simple and economical method for the biosynthesis of zinc oxide nanoparticles using different plant parts of *B. orellana* followed by their characterization using different techniques. The remarkable difference in the physicochemical properties of ZnO nanoparticles underlines the role of different biomolecules from plant extracts in synthesis of ZnO nanoparticles. L-ZnO, S-ZnO, and Sc-ZnO showed weak antibacterial properties before calcination. No antibacterial activity was observed in all three L-ZnO, S-ZnO, and Sc-ZnO nanoparticles after calcination. Non-antifungal nature of L-ZnO, S-ZnO, and Sc-ZnO nanoparticles was observed against all four fungi before and after calcination. Lack of antimicrobial potential underlined the inert nature of the as-synthesized ZnO nanoparticles. Uncalcinated and calcined ZnO nanoparticles showed no anticancer activities against HCT-116 cancer cells. Non-antimicrobial and non-anticancer potential of ZnO nanoparticles thus makes it a suitable candidate to be used as a carrier molecule for drug delivery applications. More research on zinc oxide nanoparticles is needed to explore the role of different biomolecules in the biosynthesis of ZnO nanoparticles and their potential use in biomedical applications.

4. EXPERIMENTAL SECTION

4.1. Materials Used. Zinc acetate dihydrate and ammonia were procured from Merck, India. Nutrient broth used for growing of bacterial cultures and Sabouraud's dextrose broth

https://doi.org/10.1021/acsomega.1c05324
ACS Omega 2022, 7, 1914−1933

used for growing fungal cultures and nutrient agar used for estimation of antibacterial activity and Sabouraud's dextrose agar used for estimation of antifungal activity were purchased from Himedia, India. Phosphate buffered saline (PBS) tablets, Dulbecco's modified Eagle medium (DMEM), fetal bovine serum (FBS), and 0.4% trypan blue solution were purchased from Thermo Fisher Scientific, India. All analytical grade chemicals were utilized as received without any additional purification. Milli-Q water was used for all the experimental procedures.

4.2. Preparation of *B. orellana* Leaf, Seed, and Seed Coat Extracts. Leaves, seeds, and seed coats of *B. orellana* were washed with double distilled water after which 2−3 washes were given with Milli-Q water. 250 g of leaves/seeds/seed coats were added into capped glass bottles with 1000 mL Milli-Q water which were further subjected to heating in a boiling water bath for duration of 5 min after which it was evenly swirled and further cooled down at room temperature. The leaf, seed. and seed coat extracts obtained after heating were filtered using eight-fold muslin cloth once the extract cooled down so as to obtain a clear filtrate.

4.3. Biosynthesis of Zinc Oxide Nanoparticles. Zinc acetate dihydrate was added to Milli-Q water to prepare 1.5 L of 0.05 M zinc acetate solution in individual glass bottles. 750 mL of leaf, seed and seed coat extracts were then separately added into the reaction mixture under stirring conditions at 1000 rpm followed by addition of 30 mL of ammonia until a pale yellowish to brown precipitate was observed. The reaction was kept overnight under static conditions at room temperature. The pale yellow to brownish colored precipitate settled down and the clear supernatant was slowly discarded and the precipitate was collected. The precipitate was further separated by centrifugation at 12,000 rpm for a time period of 12 min. 2−3 washes were given using Milli-Q water by centrifugation at 8000 rpm for duration of 8 min. Pellets recovered after centrifugation were then divided into two parts, one of which was air -dried and the other was subjected to calcination at 900 °C for 2 h to obtain ZnO nanoparticles. Both the uncalcinated and calcined nanoparticles were further characterized.

4.4. Characterization Techniques. The optical properties of ZnO nanoparticles biosynthesized using leaf, seed, and seed coat extracts of *B. orellana* were analyzed with the help of UV−vis spectrometric studies using a Shimadzu dual-beam spectrophotometer, model UV-1800, 240 V in the range 300−1100 nm and PL studies were carried out with the help of a Jasco spectrofluorometer FP-8300 within the range 200−750 nm. XRD analysis was conducted with the help of Rigaku Ultima IV X-ray diffractometer operating with 1.54 Å Cu K_α radiations with 2θ values within the range 30−80° with 0.005 s^{-1} scanning speed. XPS was conducted with standard conditions using Thermo Fisher ESCALAB Xi+. Morphologies of these nanoparticles have been analyzed by FESEM and TEM. FESEM analysis was performed with the help of JEOL JSM-6360A with 20 kV accelerating voltage. The elemental analysis of ZnO nanoparticles was conducted by EDS with standard conditions using Bruker XFlash 6I30. TEM analysis was performed using a JEOL JEM 2100 PLUS with 200 kV accelerating voltage. BET surface area was conducted by N_2 physisorption on a Quantachrome NOVA touch absorption analyzer from relative pressure (P/P_0) 0 to 1. The samples (∼0.5 g) were dried at 110 °C in the oven and then degassed for at least 3 h at 150 °C under vacuum prior to analysis. ATR-IR of ZnO nanoparticles, zinc acetate used as a zinc precursor salt and leaf, seed, and seed coat extracts of *B. orellana* was performed using a Shimadzu ATR-IR spectrophotometer FTIR-8400 ranging from 4000 to 400 cm^{-1}. GC−MS analysis of methanolic leaf, seed, and seed coat extracts of *B. orellana* was performed using Shimatzu, GC 2010 Plus for determining the plausible molecules. HR-MS analysis was performed where 5 μL aliquots of the aqueous leaf, seed, and seed coat extracts of *B. orellana* was directly infused into the electrospray ionization (ESI) chamber at a flow rate of 120 μL per minute. The mass spectra so obtained were then recorded using a Bruker impact HD Q-TOF spectrometer (Bruker Daltonics, Billerica, MA, USA). The mass spectrometric analysis has been performed using parameters ESI as the source type with active focus. The molecules within the range of 50−500 m/z ratio were scanned. Ion polarity was set to be positive with set capillary at 3500 V, set end plate offset at −500 V and set charging voltage at 2000 V. The set nebulizer was at 0.3 bar with a set dry heater at 200 °C and set dry gas at a rate 4.0 L per minute. The spectra were visualized followed by baseline-correction with the help of the software Bruker compass Data Analysis 4.2. NMR analysis was also performed for determining the plausible molecules in these extracts using the solvent deuterium oxide (D_2O) with the help of Bruker Ascend 400 MHz.

4.5. Micro-organisms. Gram positive (*S. aureus*, *B. subtilis*) along with Gram negative (*E. coli*, *P. aeruginosa*) microorganisms were acquired from the Microbiology Dept., S. P. Pune University, Pune, India. The bacterial cell cultures were streaked on nutrient agar slants and were preserved at temperature 4 °C with periodic sub-culturing twice a month for maintenance of bacterial cell viability. Different fungal cultures (*Penicillium* spp., *A. flavus*, *F. oxysporum*, *R. solani*) were obtained from Botany Dept., S. P. Pune University, Pune, India. Sabouraud's dextrose agar slants were streaked using fungal spore suspension and were preserved at temperature 4 °C with periodic sub-culturing every month for maintenance of fungal cell viability.

4.6. Cancer Cell Lines. HCT-116 human colorectal carcinoma cell line was procured from the National Centre for Cell Sciences (NCCS), Pune, India. The HCT-116 cancer cells were cultured using DMEM with 10% FBS. They were maintained at sterilized condition in a CO_2 incubator (5%) at a temperature of 37 °C. Once these cells reach 80% confluency, they were further sub-cultured.

4.7. Estimation of Antibacterial Properties. Antibacterial potential of ZnO nanoparticles was estimated using Gram positive and Gram negative bacteria where *S. aureus* and *B. subtilis* were taken as characteristic Gram positive bacteria whereas *E. coli* and *P. aeruginosa* were taken as characteristic Gram negative microorganisms. These microorganisms were used to test the antibacterial potential of ZnO nanoparticles biosynthesized using leaf, seed, and seed coat extracts of *B. orellana* before and after calcination within the concentration range of 0.625−10 mg/mL using well diffusion method. Inoculation was done using one bacterial colony in 5 mL of nutrient broth which was allowed to grow overnight at 37 °C under stirring conditions of 120 rpm in shaker incubator. 1% inoculum was used from the primary culture to re-inoculate in 10 mL nutrient broth which was allowed to grow at 37 °C, 150 rpm upto 0.5 McFarland's Standard. The broth containing bacterial cells was further diluted with physiological saline to a final concentration of 10^5 CFU/mL. 100 μL bacterial cultures were spread on nutrient agar Petri plates using glass spreader.

https://doi.org/10.1021/acsomega.1c05324
ACS Omega 2022, 7, 1914−1933

Nutrient agar plates were then punctured with the help of cork borer with a diameter of 5 mm to form wells. Both the calcined and uncalcinated ZnO nanoparticles were dispersed using Milli-Q water as the solvent at concentrations ranging from 0.625 to 10 mg/mL using sonication. 50 μL ZnO nanoparticles' suspension was further added into these wells followed by incubation at room temperature for 30 min for ensuring appropriate diffusion. After overnight incubation of the nutrient agar plates with bacteria and ZnO nanoparticles at 37 °C, zones of inhibition were recorded.

4.8. Estimation of Antifungal Properties. Antifungal potential of ZnO nanoparticles was estimated using different fungal cultures (*Penicillium* spp., *A. flavus*, *F. oxysporum*, *R. solani*). These fungal cultures were used to test the antifungal potential of ZnO nanoparticles biosynthesized using leaf, seed, and seed coat extracts of *B. orellana* before and after calcination at a concentration of 10 mg/mL using well diffusion method. A 1 mm square of Sabouraud's dextrose agar containing fungal inoculum was cut using sterile blade from a fully confluent fungal culture which was transferred to a fresh Sabouraud's dextrose agar Petri plate and allowed to grow at a temperature of 30 °C till full confluency was reached. A 1 mm square of Sabouraud's dextrose agar containing fungal inoculum was then cut from the freshly grown fungal culture and was further tweezed after addition of 1 mL physiological saline so as to release fungal spores. Fungal spore counting was conducted using a haemocytometer. Fungal spore suspension was then diluted with physiological saline to a final concentration of 10^4−10^5 CFU/mL. 100 μL fungal spore suspension cultures were spread on Sabouraud's dextrose agar Petri plates using glass spreader. Sabouraud's dextrose agar plates were then punctured with the help of cork borer with a diameter of 5 mm to form wells. Both the calcined and uncalcinated ZnO nanoparticles were dispersed using Milli-Q water as the solvent at a final concentration of 10 mg/mL using sonication. 50 μL ZnO nanoparticles' suspension was further added into these wells followed by incubation at room temperature for 30 min for ensuring appropriate diffusion. These Sabouraud's dextrose agar plates with fungal cultures and ZnO nanoparticles were incubated at 30 °C for 4−8 days after which zones of inhibition were recorded.

4.9. Cytotoxicity Studies. HCT-116 cancer cells were treated with 100 μg/mL ZnO nanoparticles (L-ZnO, S-ZnO, Sc-ZnO) and *B. orellana* leaf, seed, and seed coat extracts. Cells were seeded in a 96-well plate at density of 5000 cells/well and grown overnight in humidified CO_2 incubator in a total of 200 μL DMEM containing 10% FBS medium. Subsequently, cells were treated with ZnO nanoparticles and extracts in triplicate wells for 48 h. For detection of cell death, cells were treated with 40 μL 0.4% trypan blue solution diluted in 1× PBS in 1:1 ratio for 20 s. Cells were then washed with PBS solution to remove excess trypan blue solution. The phase contrast images were acquired and visualized for presence of cell death using Magvision software for image processing.

■ ASSOCIATED CONTENT

Supporting Information

The Supporting Information is available free of charge at https://pubs.acs.org/doi/10.1021/acsomega.1c05324.

EDS analysis of L-ZnO, S-ZnO, and Sc-ZnO nanoparticles and GC−MS, HR-MS, and NMR analysis of BL, BS, and BSc extracts (PDF)

■ AUTHOR INFORMATION

Corresponding Author

Balaprasad Ankamwar − *Bio-Inspired Materials Research Laboratory, Department of Chemistry, Savitribai Phule Pune University (Formerly University of Pune), Pune 411007, India;* orcid.org/0000-0002-9986-6298; Email: sb180305@gmail.com

Authors

Saee Gharpure − *Bio-Inspired Materials Research Laboratory, Department of Chemistry, Savitribai Phule Pune University (Formerly University of Pune), Pune 411007, India*

Rachana Yadwade − *Bio-Inspired Materials Research Laboratory, Department of Chemistry, Savitribai Phule Pune University (Formerly University of Pune), Pune 411007, India*

Complete contact information is available at: https://pubs.acs.org/10.1021/acsomega.1c05324

Author Contributions

S.G. and R.Y. contributed equally. BA designed the concept and outline of the experimental work. The experimental work was performed by all authors and manuscript was written through contributions of all authors. All authors have given approval to the final version of the manuscript.

Funding

There was no funding received for this research from any of the funding bodies.

Notes

The authors declare no competing financial interest.

■ ACKNOWLEDGMENTS

S.G. and R.Y. are obliged towards Department of Chemistry, Savitribai Phule Pune University for providing the opportunity to work for the Ph.D. degree under the guidance of B.A. All the co-authors would like to extend their gratitude to Dr. Karishma Pardesi, Microbiology Dept., S. P. Pune University for providing bacterial cultures and Dr. Mahesh Borde, Botany Dept., S. P. Pune University for providing fungal cultures. All the co-authors would like to acknowledge Shreeram Sahasrabuddhe for providing with the leaves, seeds and seed coats of *B. orellana* plant source growing in his backyard for this study.

■ ABBREVIATIONS

BL, *Bixa orellana* leaf; BS, *Bixa orellana* seed; BSc, *Bixa orellana* seed coat; ZnO, zinc oxide; BC, before calcination; AC, after calcination; L-ZnO, zinc oxide nanoparticles synthesized using *Bixa orellana* leaf extract; S-ZnO, zinc oxide nanoparticles synthesized using *Bixa orellana* seed extract; Sc-ZnO, zinc oxide nanoparticles synthesized using *Bixa orellana* seed coat extract

■ REFERENCES

(1) Cassini, A.; Högberg, L. D.; Plachouras, D.; Quattrocchi, A.; Hoxha, A.; Simonsen, G. S.; Colomb-Cotinat, M.; Kretzschmar, M. E.; Devleesschauwer, B.; Cecchini, M.; Ouakrim, D. A.; Oliveira, T. C.; Struelens, M. J.; Suetens, C.; Monnet, D. L.; Strauss, R.; Mertens, K.; Struyf, T.; Catry, B.; Latour, K.; Ivanov, I. N.; Dobreva, E. G.; Tambic Andraševic, A.; Soprek, S.; Budimir, A.; Paphitou, N.; Žemlicková, H.; Schytte Olsen, S.; Wolff Sönksen, U.; Märtin, P.; Ivanova, M.; Lyytikäinen, O.; Jalava, J.; Coignard, B.; Eckmanns, T.; Abu Sin, M.; Haller, S.; Daikos, G. L.; Gikas, A.; Tsiodras, S.; Kontopidou, F.;

Tóth, Á.; Hajdu, Á.; Guólaugsson, Ó.; Kristinsson, K. G.; Murchan, S.; Burns, K.; Pezzotti, P.; Gagliotti, C.; Dumpis, U.; Liuimiene, A.; Perrin, M.; Borg, M. A.; de Greeff, S. C.; Monen, J. C.; Koek, M. B.; Elstrøm, P.; Zabicka, D.; Deptula, A.; Hryniewicz, W.; Caniça, M.; Nogueira, P. J.; Fernandes, P. A.; Manageiro, V.; Popescu, G. A.; Serban, R. I.; Schréterová, E.; Litvová, S.; Štefkovicová, M.; Kolman, J.; Klavs, I.; Korošec, A.; Aracil, B.; Asensio, A.; Pérez-Vázquez, M.; Billström, H.; Larsson, S.; Reilly, J. S.; Johnson, A.; Hopkins, S. Attributable Deaths and Disability-adjusted Life-years Caused by Infections with Antibiotic-resistant Bacteria in the EU and the European Economic Area in 2015: A Population-level Modelling Analysis. *Lancet Infect. Dis.* **2019**, *19*, 56−66.

(2) McNeilly, O.; Mann, R.; Hamidian, M.; Gunawan, C. Emerging Concern for Silver Nanoparticle Resistance in *Acinetobacter baumannii* and Other Bacteria. *Front. Microbiol.* **2021**, *12*, 652863.

(3) Fair, R. J.; Tor, Y. Antibiotics and Bacterial Resistance in the 21st Century. *Perspect. Med. Chem.* **2014**, *6*, 25−64.

(4) Prestinaci, F.; Pezzotti, P.; Pantosti, A. Antimicrobial Resistance: A Global Multifaceted Phenomenon. *Pathog. Global Health* **2015**, *109*, 309−318.

(5) Wang, L.; Hu, C.; Shao, L. The Antimicrobial Activity of Nanoparticles: Present Situation and Prospects for the Future. *Int. J. Nanomed.* **2017**, *12*, 1227−1249.

(6) Roselli, M.; Finamore, A.; Garaguso, I.; Britti, M. S.; Mengheri, E. Zinc Oxide Protects Cultured Enterocytes from the Damage Induced by *Escherichia coli*. *J. Nutr.* **2003**, *133*, 4077−4082.

(7) Maret, W. Zinc Biochemistry: From a Single Zinc Enzyme to a Key Element of Life. *Adv. Nutr.* **2013**, *4*, 82−91.

(8) Halbus, A. F.; Horozov, T. S.; Paunov, V. N. Surface-Modified Zinc Oxide Nanoparticles for Antialgal and Antiyeast Applications. *ACS Appl. Nano Mater.* **2020**, *3*, 440−451.

(9) Dikshit, P.; Kumar, J.; Das, A.; Sadhu, S.; Sharma, S.; Singh, S.; Gupta, P.; Kim, B. Green Synthesis of Metallic Nanoparticles: Applications and Limitations. *Catalysts* **2021**, *11*, 902.

(10) Raghupathi, K. R.; Koodali, R. T.; Manna, A. C. Size-dependent Bacterial Growth Inhibition and Mechanism of Antibacterial Activity of Zinc Oxide Nanoparticles. *Langmuir* **2011**, *27*, 4020−4028.

(11) Lipovsky, A.; Nitzan, Y.; Gedanken, A.; Lubart, R. Antifungal Activity of ZnO Nanoparticles—the Role of ROS Mediated Cell Injury. *Nanotechnology* **2011**, *22*, 105101.

(12) Sirelkhatim, A.; Mahmud, S.; Seeni, A.; Kaus, N. H. M.; Ann, L. C.; Bakhori, S. K. M.; Hasan, H.; Mohamad, D. Review on Zinc Oxide Nanoparticles: Antibacterial Activity and Toxicity Mechanism. *Nano-Micro Lett.* **2015**, *7*, 219−242.

(13) Galván Márquez, I.; Ghiyasvand, M.; Massarsky, A.; Babu, M.; Samanfar, B.; Omidi, K.; Moon, T. W.; Smith, M. L.; Golshani, A. Zinc Oxide and Silver Nanoparticles Toxicity in the Baker's Yeast, *Saccharomyces cerevisiae*. *PLoS One* **2018**, *13*, No. e0193111.

(14) He, L.; Liu, Y.; Mustapha, A.; Lin, M. Antifungal Activity of Zinc Oxide Nanoparticles against *Botrytis cinerea* and *Penicillium expansum*. *Microbiol. Res.* **2011**, *166*, 207−215.

(15) Rago, I.; Chandraiahgari, C. R.; Bracciale, M. P.; De Bellis, G.; Zanni, E.; Cestelli Guidi, M.; Sali, D.; Broggi, A.; Palleschi, C.; Sarto, M. S.; Uccelletti, D. Zinc Oxide Microrods and Nanorods: Different Antibacterial Activity and their Mode of Action against Gram-positive Bacteria. *RSC Adv.* **2014**, *4*, 56031−56040.

(16) Bodar, C. W. M.; Pronk, M. E. J.; Sijm, D. T. H. M. The European Union Risk Assessment on Zinc and Zinc Compounds: The Process and the Facts. *Integr. Environ. Assess. Manage.* **2005**, *1*, 301−319.

(17) Mohd Yusof, H.; Abdul Rahman, N. A.; Mohamad, R.; Zaidan, U. H.; Samsudin, A. A. Biosynthesis of Zinc Oxide Nanoparticles by Cell-Biomass and Supernatant of *Lactobacillus plantarum* TA4 and its Antibacterial and Biocompatibility Properties. *Sci. Rep.* **2020**, *10*, 19996.

(18) Khan, A. K.; Renouard, S.; Drouet, S.; Blondeau, J.-P.; Anjum, I.; Hano, C.; Abbasi, B. H.; Anjum, S. Effect of UV Irradiation (A and C) on *Casuarina equisetifolia*-Mediated Biosynthesis and Characterization of Antimicrobial and Anticancer Activity of Biocompatible Zinc Oxide Nanoparticles. *Pharmaceutics* **2021**, *13*, 1977.

(19) Tettey, C. O.; Shin, H. M. Evaluation of the Antioxidant and Cytotoxic Activities of Zinc Oxide Nanoparticles Synthesized using *Scutellaria baicalensis* Root. *Sci. Afr.* **2019**, *6*, No. e00157.

(20) Wang, C.; Lu, J.; Zhou, L.; Li, J.; Xu, J.; Li, W.; Zhang, L.; Zhong, X.; Wang, T. Effects of Long-term Exposure to Zinc Oxide Nanoparticles on Development, Zinc Metabolism and Biodistribution of Minerals (Zn, Fe, Cu, Mn) in Mice. *PLoS One* **2016**, *11*, No. e0164434.

(21) Naahidi, S.; Jafari, M.; Edalat, F.; Raymond, K.; Khademhosseini, A.; Chen, P. Biocompatibility of Engineered Nanoparticles for Drug Delivery. *J. Controlled Release* **2013**, *166*, 182−194.

(22) S, M.; N, H.; P.P, V. In vitro Biocompatibility and Antimicrobial Activities of Zinc Oxide Nanoparticles (ZnO NPs) Prepared by Chemical and Green Synthetic Route—A Comparative Study. *J. Bionanosci.* **2020**, *10*, 112−121.

(23) Happy Agarwal, H.; Soumya Menon, S.; Venkat Kumar, S.; Rajeshkumar, S. Mechanistic Study on Antibacterial Action of Zinc Oxide Nanoparticles Synthesized Using Green Route. *Chem.-Biol. Interact.* **2018**, *286*, 60−70.

(24) Ijaz, I.; Gilani, E.; Nazir, A.; Bukhari, A. Detail Review on Chemical, Physical and Green Synthesis, Classification, Characterizations and Applications of Nanoparticles. *Green Chem. Lett. Rev.* **2020**, *13*, 223−245.

(25) Shaba, E. Y.; Jacob, J. O.; Tijani, J. O.; Suleiman, M. A. T. A Critical Review of Synthesis Parameters Affecting the Properties of Zinc Oxide Nanoparticle and its Application in Wastewater Treatment. *Appl. Water Sci.* **2021**, *11*, 48.

(26) Fakhari, S.; Jamzad, M.; Kabiri Fard, H. Green Synthesis of Zinc Oxide Nanoparticles: A Comparison. *Green Chem. Lett. Rev.* **2019**, *12*, 19−24.

(27) Wiesmann, N.; Tremel, W.; Brieger, J. Zinc Oxide Nanoparticles for Therapeutic Purposes in Cancer Medicine. *J. Mater. Chem. B* **2020**, *8*, 4973−4989.

(28) Basnet, P.; Inakhunbi Chanu, T.; Samanta, D.; Chatterjee, S. A Review on Bio-synthesized Zinc Oxide Nanoparticles Using Plant Extracts as Reductants and Stabilizing Agents. *J. Photochem. Photobiol., B* **2018**, *183*, 201−221.

(29) Jayappa, M. D.; Ramaiah, C. K.; Kumar, M. A. P.; Suresh, D.; Prabhu, A.; Devasya, R. P.; Sheikh, S. Green Synthesis of Zinc Oxide Nanoparticles from the Leaf, Stem and In vitro Grown Callus of *Mussaenda frondosa* L.: Characterization and their Applications. *Appl. Nanosci.* **2020**, *10*, 3057−3074.

(30) Shahid-ul-Islam, L. J.; Rather, L. J.; Mohammad, F. Phytochemistry, Biological Activities and Potential of Annatto in Natural Colorant Production for Industrial Applications−A Review. *J. Adv. Res.* **2016**, *7*, 499−514.

(31) Naseer, M.; Aslam, U.; Khalid, B.; Chen, B. Green route to synthesize Zinc Oxide Nanoparticles using Leaf Extracts of *Cassia fistula* and *Melia azadarach* and their Antibacterial Potential. *Sci. Rep.* **2020**, *10*, 9055.

(32) Sadiq, H.; Sher, F.; Sehar, S.; Lima, E. C.; Zhang, S.; Iqbal, H. M. N.; Zafar, F.; Nuhanović, M. Green Synthesis of ZnO Nanoparticles from *Syzygium cumini* Leaves Extract with Robust Photocatalysis Applications. *J. Mol. Liq.* **2021**, *335*, 116567.

(33) Kalpana, V. N.; Kataru, B. A. S.; Sravani, N.; Vigneshwari, T.; Panneerselvam, A.; Devi Rajeswari, V. Biosynthesis of Zinc Oxide Nanoparticles Using Culture Filtrates of *Aspergillus niger*: Antimicrobial Textiles and Dye Degradation Studies. *OpenNano* **2018**, *3*, 48−55.

(34) Rajendran, N. K.; George, B. P.; Houreld, N. N.; Abrahamse, H. Synthesis of Zinc Oxide Nanoparticles Using *Rubus fairholmianus* Root Extract and Their Activity against Pathogenic Bacteria. *Molecules* **2021**, *26*, 3029.

(35) Farhadi-Khouzani, M.; Fereshteh, Z.; Loghman-Estarki, M. R.; Razavi, R. S. Different morphologies of ZnO nanostructures via

https://doi.org/10.1021/acsomega.1c05324
ACS Omega 2022, 7, 1914−1933

polymeric complex sol−gel method: synthesis and characterization. *J. Sol-Gel Sci. Technol.* **2012**, *64*, 193−199.
(36) Dolcet, P.; Casarin, M.; Maccato, C.; Bovo, L.; Ischia, G.; Gialanella, S.; Mancin, F.; Tondello, E.; Gross, S. Miniemulsions as Chemical Nanoreactors for the Room Temperature Synthesis of Inorganic Crystalline Nanostructures: ZnO Colloids. *J. Mater. Chem.* **2012**, *22*, 1620−1626.
(37) Zak, A. K.; Abrishami, M. E.; Majid, W. H. A.; Yousefi, R.; Hosseini, S. M. Effects of Annealing Temperature on Some Structural and Optical Properties of ZnO Nanoparticles Prepared by a Modified Sol−gel Combustion Method. *Ceram. Interfaces* **2011**, *37*, 393−398.
(38) Pradeev raj, K.; Sadaiyandi, K.; Kennedy, A.; Sagadevan, S.; Chowdhury, Z. Z.; Johan, M. R. B.; Aziz, F. A.; Rafique, R. F.; Thamiz Selvi, R.; Rathina bala, R. Influence of Mg Doping on ZnO Nanoparticles for Enhanced Photocatalytic Evaluation and Antibacterial Analysis. *Nanoscale Res. Lett.* **2018**, *13*, 229.
(39) Husain, F. M.; Ahmad, I.; Al-Thubiani, A. S.; Abulreesh, H. H.; AlHazza, I. M.; Aqil, F. Leaf Extracts of *Mangifera indica* L. Inhibit Quorum Sensing−Regulated Production of Virulence Factors and Biofilm in Test Bacteria. *Front. Microbiol.* **2017**, *8*, 727.
(40) Kumar Jangir, L.; Kumari, Y.; Kumar, A.; Kumar, M.; Awasthi, K. Investigation of Luminescence and Structural Properties of ZnO Nanoparticles, Synthesized With Different Precursors. *Mater. Chem. Front.* **2017**, *1*, 1413−1421.
(41) Sundarakannan, B.; Kottaisamy, M. Blue Light Excitable Red Emitting ZnO and its Blend For High CRI White Light Emitting Diodes Applications. *J. Lumin.* **2022**, *241*, 118447.
(42) Raoufi, D. Synthesis and Photoluminescence Characterization of ZnO Nanoparticles. *J. Lumin.* **2013**, *134*, 213−219.
(43) Lopes de Almeida, W.; Ferreira, N. S.; Rodembusch, F. S.; Caldas de Sousa, V. Study of Structural and Optical Properties of ZnO Nanoparticles Synthesized By An Eco-friendly Tapioca-Assisted Route. *Mater. Chem. Phys.* **2021**, *258*, 123926.
(44) Veerabhadraiah, S. R.; Maji, S.; Panneerselvam, A. Solvent Influence on the Formation of ZnO Nanoparticles by Sonochemical Technique and Evaluation of UV-Blocking Efficiency. *J. Cryst. Growth* **2022**, *579*, 126430.
(45) Bandi, V. R.; Nien, Y.-T.; Lu, T.-H.; Chen, I.-G. Effect of Calcination Temperature and Concentration on Luminescence Properties of Novel $Ca_3Y_2Si_3O_{12}$:Eu Phosphors. *J. Am. Ceram. Soc.* **2009**, *92*, 2953−2956.
(46) Somasundaram, G.; Rajan, J.; Paul, J. Effect of the Calcination Process on CdO−ZnO Nanocomposites by a Honey-Assisted Combustion Method for Antimicrobial Performance. *Toxicol. Res.* **2018**, *7*, 779−791.
(47) Shim, E. S.; Kang, H. S.; Pang, S. S.; Kang, J. S.; Yun, I.; Lee, S. Y. Annealing Effect on the Structural and Optical Properties of ZnO Thin Film on InP. *Mater. Sci. Eng., B* **2003**, *102*, 366−369.
(48) Chitradevi, T.; Jestin Lenus, A.; Victor Jaya, N. Structure, Morphology and Luminescence Properties of Sol-gel Method Synthesized Pure and Ag-doped ZnO Nanoparticles. *Mater. Res. Express* **2019**, *7*, 015011.
(49) Sunkara, P.; Masula, K.; Puppala, V.; Bhongiri, Y.; Pasala, V. K.; Basude, M. Highly Active Zinc Oxide-Supported Lithium Oxide Catalyst for Solvent-Free Knoevenagel Condensation. *J. Chem. Sci.* **2021**, *133*, 67.
(50) Mclaren, A.; Valdes-Solis, T.; Li, G.; Tsang, S. C. Shape and Size Effects of ZnO Nanocrystals on Photocatalytic Activity. *J. Am. Chem. Soc.* **2009**, *131*, 12540−12541.
(51) Factori, I. M.; Amaral, J. M.; Camani, P. H.; Rosa, D. S.; Lima, B. A.; Brocchi, M.; da Silva, E. R.; Souza, J. S. ZnO Nanoparticle/Poly (vinyl alcohol) Nanocomposites via Microwave-Assisted Sol−Gel Synthesis for Structural Materials, UV Shielding, and Antimicrobial Activity. *ACS Appl. Nano Mater.* **2021**, *4*, 7371−7383.
(52) Sulciute, A.; Nishimura, K.; Gilshtein, E.; Cesano, F.; Viscardi, G.; Nasibulin, A. G.; Ohno, Y.; Rackauskas, S. ZnO Nanostructures Application in Electrochemistry: Influence of Morphology. *J. Phys. Chem. C* **2021**, *125*, 1472−1482.
(53) Wohlleben, W.; Ma-Hock, L.; Boyko, V.; Cox, G.; Egenolf, H.; Freiberger, H.; Hinrichsen, B.; Hirth, S.; Landsiedel, R. Nanospecific Guidance in REACH: A Comparative Physical-chemical Characterization of 15 Materials with Methodical Correlations. *J. Ceramic Sci. Technol.* **2013**, *4*, 93−104.
(54) Bushell, M.; Beauchemin, S.; Kunc, F.; Gardner, D.; Ovens, J.; Toll, F.; Kennedy, D.; Nguyen, K.; Vladisavljevic, D.; Rasmussen, P. E.; Johnston, L. J. Characterization of Commercial Metal Oxide Nanomaterials: Crystalline Phase, Particle Size and Specific Surface Area. *Nanomaterials* **2020**, *10*, 1812.
(55) Islam, M. T.; Dominguez, A.; Alvarado-Tenorio, B.; Bernal, R. A.; Montes, M. O.; Noveron, J. C. Sucrose-mediated Fast Synthesis of Zinc Oxide Nanoparticles for the Photocatalytic Degradation of Organic Pollutants in Water. *ACS Omega* **2019**, *4*, 6560−6572.
(56) Krzywiecki, M.; Grządziel, L.; Sarfraz, A.; Iqbal, D.; Szwajca, A.; Erbe, A. Zinc oxide as a Defect-dominated Material in Thin Films for Photovoltaic Applications−Experimental Determination of Defect Levels, Quantification of Composition, and Construction of Band Diagram. *Phys. Chem. Chem. Phys.* **2015**, *17*, 10004−10013.
(57) Al-Gaashani, R.; Radiman, S.; Daud, A. R.; Tabet, N.; Al-Douri, Y. XPS and Optical Studies of Different Morphologies of ZnO Nanostructures Prepared by Microwave Methods. *Ceram. Int.* **2013**, *39*, 2283−2292.
(58) Das, J.; Pradhan, S. K.; Sahu, D. R.; Mishra, D. K.; Sarangi, S. N.; Nayak, B. B.; Verma, S.; Roul, B. K. Micro-Raman and XPS Studies of Pure ZnO Ceramics. *Phys. B* **2010**, *405*, 2492−2497.
(59) Rakshit, T.; Mondal, S. P.; Manna, I.; Ray, S. K. CdS-Decorated ZnO Nanorod Heterostructures for Improved Hybrid Photovoltaic Devices. *ACS Appl. Mater. Interfaces* **2012**, *4*, 6085−6095.
(60) Kovačič, S.; Anžlovar, A.; Erjavec, B.; Kapun, G.; Matsko, N. B.; Žigon, M.; Žagar, E.; Pintar, A.; Slugovc, C. Macroporous ZnO Foams by High Internal Phase Emulsion Technique: Synthesis and Catalytic Activity. *ACS Appl. Mater. Interfaces* **2014**, *6*, 19075−19081.
(61) Shah, N. N. H.; Misran, H.; Razak, N. A. A.; Salim, M. A.; Othman, S. Z.; Manap, A. Modified combustion synthesis of ZnO nanoparticles using renewable fuel. *IOP Conf. Ser.: Earth Environ. Sci.* **2013**, *16*, 012038.
(62) Farzana, R.; Rajarao, R.; Hassan, K.; Behera, P. R.; Sahajwalla, V. Thermal Nanosizing: Novel Route to Synthesize Manganese Oxide and Zinc Oxide Nanoparticles Simultaneously from Spent Zn−C Battery. *J. Cleaner Prod.* **2018**, *196*, 478−488.
(63) Tharsika, T.; Haseeb, A. S. M. A.; Akbar, S. A.; Thanihaichelvan, M. Tailoring ZnO Nanostructures by Spray Pyrolysis and Thermal Annealing. *Ceram. Int.* **2015**, *41*, 5205−5211.
(64) Šćepanović, M.; Grujić-Brojčin, M.; Vojisavljević, K.; Bernik, S.; Srećković, T. Raman Study of Structural Disorder in ZnO Nanopowders. *J. Raman Spectrosc.* **2010**, *41*, 914−921.
(65) Geetha, M. S.; Nagabhushana, H.; Shivananjaiah, H. N. Green Mediated Synthesis and Characterization of ZnO Nanoparticles Using *Euphorbia Jatropa* Latex as Reducing Agent. *J. Sci.: Adv. Mater. Devices* **2016**, *1*, 301−310.
(66) Devi Chandra, R.; Gopchandran, K. G. Simple, Low-Temperature Route to Synthesize ZnO Nanoparticles and Their Optical Neuromorphic Characteristics. *ACS Appl. Electron. Mater.* **2021**, *3*, 3846−3854.
(67) Medina, J.; Bolaños, H.; Mosquera-Sanchez, L. P.; Rodriguez-Paez, J. E. Controlled Synthesis of ZnO Nanoparticles and Evaluation of their Toxicity in *Mus musculus* Mice. *Int. Nano Lett.* **2018**, *8*, 165−179.
(68) Patterson, S.; Arora, P.; Price, P.; Dittmar, J. W.; Das, V. K.; Pink, M.; Stein, B.; Morgan, D. G.; Losovyj, Y.; Koczkur, K. M.; Skrabalak, S. E.; Bronstein, L. M. Oriented Attachment is a Major Control Mechanism to Form Nail-like Mn-doped ZnO Nanocrystals. *Langmuir* **2017**, *33*, 14709−14717.
(69) Ponnusamy, R.; Sivasubramanian, D.; Sreekanth, P.; Gandhiraj, V.; Philip, R.; Bhalerao, G. M. Nonlinear Optical Interactions of Co:ZnO Nanoparticles in Continuous and Pulsed Mode of Operations. *RSC Adv.* **2015**, *5*, 80756−80765.

https://doi.org/10.1021/acsomega.1c05324
ACS Omega 2022, 7, 1914−1933

(70) Mudusu, D.; Nandanapalli, K. R.; Dugasani, S. R.; Park, S. H.; Tu, C. W. Zinc Oxide Nanorods Shielded with an Ultrathin Nickel Layer: Tailoring of Physical Properties. *Sci. Rep.* **2016**, *6*, 28561.
(71) Vogel, A. I.; Tatchell, A. R.; Furnis, B. S.; Hannaford, A. J.; Smith, P. W. *Vogel's Textbook of Practical Organic Chemistry*; John Wiley & Sons, Inc.: New York, 1989.
(72) Silverstein, R. M.; Bassler, G. C. Spectrometric Identification of Organic Compounds. *J. Chem. Educ.* **1962**, *39*, 546−553.
(73) Sarkar, J.; Ghosh, M.; Mukherjee, A.; Chattopadhyay, D.; Acharya, K. Biosynthesis and Safety Evaluation of ZnO Nanoparticles. *Bioprocess Biosyst. Eng.* **2014**, *37*, 165−171.
(74) Balraj, B.; Senthilkumar, N.; Siva, C.; Krithikadevi, R.; Julie, A.; Potheher, I. V.; Arulmozhi, M. Synthesis and Characterization of Zinc Oxide Nanoparticles Using Marine *Streptomyces sp*. with its Investigations on Anticancer and Antibacterial Activity. *Res. Chem. Intermed.* **2017**, *43*, 2367−2376.
(75) Reyes-García, L.; Lizama, F.; Roldan, V.; Troncoso, C.; Flores, M. Coupled Gas Chromatographic-Electroantennographic Responses of *Xanthogaleruca luteola* (Müller)(Coleoptera: Chrysomelidae) to Volatile Organic Compounds from *Eucalyptus globulus* Extract. *Chil. J. Agric. Res.* **2021**, *81*, 119−125.
(76) He, Y.; Li, Z.; Wang, W.; Sooranna, S.; Shi, Y.; Chen, Y.; Wu, C.; Zeng, J.; Tang, Q.; Xie, H. Chemical Profiles and Simultaneous Quantification of *Aurantii fructus* by Use of HPLC-Q-TOF-MS Combined with GC-MS and HPLC Methods. *Molecules* **2018**, *23*, 2189.
(77) Mariani, C.; Cesa, S.; Ingallina, C.; Mannina, L. Identification of tetrahydrogeranylgeraniol and dihydrogeranylgeraniol in extra virgin olive oil. *Grasas Aceites* **2018**, *69*, 263.
(78) Dwivedi, M. K.; Sonter, S.; Mishra, S.; Singh, P.; Singh, P. K. Secondary metabolite profiling and characterization of diterpenes and flavones from the methanolic extract of *Andrographis paniculata* using HPLC-LC-MS/MS. *Future J. Pharm. Sci.* **2021**, *7*, 184.
(79) Nakakuni, M.; Yamasaki, Y.; Yoshitake, N.; Takehara, K.; Yamamoto, S. Methyl Ether-Derivatized Sterols and Coprostanol Produced via Thermochemolysis Using Tetramethylammonium Hydroxide (TMAH). *Molecules* **2019**, *24*, 4040.
(80) Sopoušek, J.; Pinkas, J.; Brož, P.; Buršík, J.; Vykoukal, V.; Škoda, D.; Stýskalík, A.; Zobač, O.; Vřešťál, J.; Hrdlička, A.; Šimbera, J. Ag-Cu colloid synthesis: bimetallic nanoparticle characterisation and thermal treatment. *J. Nanomater.* **2014**, *2014*, 638964.
(81) Takashima, S.; Toyoshi, K.; Yamamoto, T.; Shimozawa, N. Positional Determination of the Carbon−Carbon Double Bonds in Unsaturated Fatty Acids Mediated by Solvent Plasmatization Using LC−MS. *Sci. Rep.* **2020**, *10*, 12988.
(82) Rubel Mozumder, N. H. M.; Lee, Y.-R.; Hwang, K. H.; Lee, M.-S.; Kim, E.-H.; Hong, Y.-S. Characterization of Tea Leaf Metabolites Dependent on Tea (*Camellia sinensis*) Plant Age Through ^{1}H NMR-Based Metabolomics. *Appl. Biol. Chem.* **2020**, *63*, 10.
(83) Ward, J. L.; Baker, J. M.; Beale, M. H. Recent Applications of NMR Spectroscopy in Plant Metabolomics. *FEBS J.* **2007**, *274*, 1126−1131.
(84) Gurgur, E.; Oluyamo, S. S.; Adetuyi, A. O.; Omotunde, O. I.; Okoronkwo, A. E. Green Synthesis of Zinc Oxide Nanoparticles and Zinc Oxide−Silver, Zinc Oxide−Copper Nanocomposites Using *Bridelia ferruginea* as Biotemplate. *SN Appl. Sci.* **2020**, *2*, 911.
(85) Soto-Robles, C. A.; Nava, O. J.; Vilchis-Nestor, A. R.; Castro-Beltrán, A.; Gómez-Gutiérrez, C. M.; Lugo-Medina, E.; Olivas, A.; Luque, P. A. Biosynthesized Zinc Oxide Using *Lycopersicon esculentum* Peel Extract for Methylene Blue Degradation. *J. Mater. Sci.: Mater. Electron.* **2018**, *29*, 3722−3729.
(86) Lallo da Silva, B.; Caetano, B. L.; Chiari-Andréo, B. G.; Pietro, R. C. L. R.; Chiavacci, L. A. Increased Antibacterial Activity of ZnO Nanoparticles: Influence of Size and Surface Modification. *Colloids Surf., B* **2019**, *177*, 440−447.
(87) Aldeen, T. S.; Ahmed Mohamed, H. E.; Maaza, M. ZnO Nanoparticles Prepared via a Green Synthesis Approach: Physical Properties, Photocatalytic and Antibacterial Activity. *J. Phys. Chem. Solids* **2022**, *160*, 110313.
(88) Gupta, M.; Tomar, R. S.; Kaushik, S.; Mishra, R. K.; Sharma, D. Effective Antimicrobial Activity of Green ZnO Nanoparticles of *Catharanthus roseus*. *Front. Microbiol.* **2018**, *9*, 2030.
(89) Banoee, M.; Seif, S.; Nazari, Z. E.; Jafari-Fesharaki, P.; Shahverdi, H. R.; Moballegh, A.; Moghaddam, K. M.; Shahverdi, A. R. ZnO Nanoparticles Enhanced Antibacterial Activity of Ciprofloxacin Against *Staphylococcus aureus* and *Escherichia coli*. *J. Biomed. Mater. Res., Part B* **2010**, *93*, 557−561.
(90) Abd Elkodous, M.; El-Sayyad, G. S.; Abdel Maksoud, M. I. A.; Abdelrahman, I. Y.; Mosallam, F. M.; Gobara, M.; El-Batal, A. I. Fabrication of Ultra-pure Anisotropic Zinc Oxide Nanoparticles via Simple and Cost-effective Route: Implications for UTI and EAC Medications. *Biol. Trace Elem. Res.* **2020**, *196*, 297−317.
(91) Carofiglio, M.; Barui, S.; Cauda, V.; Laurenti, M. Doped Zinc Oxide Nanoparticles: Synthesis, Characterization and Potential Use in Nanomedicine. *Appl. Sci.* **2020**, *10*, 5194.
(92) Aditya, A.; Chattopadhyay, S.; Gupta, N.; Alam, S.; Veedu, A. P.; Pal, M.; Singh, A.; Santhiya, D.; Ansari, K. M.; Ganguli, M. ZnO Nanoparticles Modified with an Amphipathic Peptide Show Improved Photoprotection in Skin. *ACS Appl. Mater. Interfaces* **2018**, *11*, 56−72.
(93) Barua, S.; Mitragotri, S. Challenges Associated with Penetration of Nanoparticles Across Cell and Tissue Barriers: A Review of Current Status and Future Prospects. *Nano Today* **2014**, *9*, 223−243.
(94) Leung, Y. H.; Chan, C. M. N.; Ng, A. M. C.; Chan, H. T.; Chiang, M. W. L.; Djurišić, A. B.; Ng, Y. H.; Jim, W. Y.; Guo, M. Y.; Leung, F. C. C.; Chan, W. K.; Au, D. T. W. Antibacterial Activity of ZnO Nanoparticles with a Modified Surface Under Ambient Illumination. *Nanotechnology* **2012**, *23*, 475703.
(95) Ankamwar, B.; Gharpure, S. Non-antibacterial Biogenic Gold Nanoparticles an Ulterior Drug Carrier. *Mater. Res. Express* **2019**, *6*, 1050c7.
(96) Gharpure, S.; Kirtiwar, S.; Palwe, S.; Akash, A.; Ankamwar, B. Non-antibacterial as well as Non-anticancer Activity of Flower Extract and its Biogenous Silver Nanoparticles. *Nanotechnology* **2019**, *30*, 195701.
(97) Cao, D.; Shu, X.; Zhu, D.; Liang, S.; Hasan, M.; Gong, S. Lipid-Coated ZnO Nanoparticles Synthesis, Characterization and Cytotoxicity Studies in Cancer Cell. *Nano Convergence* **2020**, *7*, 14.
(98) Gordon, T.; Kopel, M.; Grinblat, J.; Banin, E.; Margel, S. New Synthesis, Characterization and Antibacterial Properties of Porous ZnO and C-ZnO Micrometre-Sized Particles of Narrow Size Distribution. *J. Mater. Chem.* **2012**, *22*, 3614−3623.
(99) Zarrindokht Emami-Karvani, Z.; Chehrazi, P. Antibacterial Activity of ZnO Nanoparticle on Gram-Positive and Gram-Negative Bacteria. *Afr. J. Microbiol. Res.* **2011**, *5*, 1368−1373.
(100) Fayaz, A. M.; Balaji, K.; Girilal, M.; Yadav, R.; Kalaichelvan, P. T.; Venketesan, R. Biogenic Synthesis of Silver Nanoparticles and their Synergistic Effect with Antibiotics: A Study Against Gram-positive and Gram-negative Bacteria. *Nanomedicine* **2010**, *6*, 103−109.
(101) Niño-Martínez, N.; Salas Orozco, M. F.; Martínez-Castañón, G.-A.; Torres Méndez, F.; Ruiz, F. Molecular Mechanisms of Bacterial Resistance to Metal and Metal Oxide Nanoparticles. *Int. J. Mol. Sci.* **2019**, *20*, 2808.
(102) Elsholz, A. K. W.; Wacker, S. A.; Losick, R. Self-Regulation of Exopolysaccharide Production in *Bacillus subtilis* by a Tyrosine Kinase. *Genes Dev.* **2014**, *28*, 1710−1720.
(103) Gudkov, S. V.; Burmistrov, D. E.; Serov, D. A.; Rebezov, M. B.; Semenova, A. A.; Lisitsyn, A. B. A Mini Review of Antibacterial Properties of ZnO Nanoparticles. *Front. Phys.* **2021**, *9*, 641481.
(104) Rai, M.; Ingle, A. P.; Paralikar, P.; Anasane, N.; Gade, R.; Ingle, P. Effective Management of Soft Rot of Ginger Caused by *Pythium spp*. and *Fusarium spp*.: Emerging Role of Nanotechnology. *Appl. Microbiol. Biotechnol.* **2018**, *102*, 6827−6839.
(105) Pariona, N.; Paraguay-Delgado, F.; Basurto-Cereceda, S.; Morales-Mendoza, J. E.; Hermida-Montero, L. A.; Mtz-Enriquez, A. I. Shape-dependent Antifungal Activity of ZnO Particles Against Phytopathogenic Fungi. *Appl. Nanosci.* **2020**, *10*, 435−443.

https://doi.org/10.1021/acsomega.1c05324
ACS Omega 2022, 7, 1914−1933

(106) Zare, E.; Pourseyedi, S.; Khatami, M.; Darezereshki, E. Simple Biosynthesis of Zinc Oxide Nanoparticles using Nature's Source, and it's in vitro Bio-activity. *J. Mol. Struct.* **2017**, *1146*, 96−103.
(107) Kalia, A.; Kaur, J.; Tondey, M.; Manchanda, P.; Bindra, P.; Alghuthaymi, M. A.; Shami, A.; Abd-Elsalam, K. A. Differential Antimycotic and Antioxidant Potentials of Chemically Synthesized Zinc-Based Nanoparticles Derived from Different Reducing/Complexing Agents against Pathogenic Fungi of Maize Crop. *J. Fungi* **2021**, *7*, 223.
(108) Sun, Q.; Li, J.; Le, T. Zinc Oxide Nanoparticle as a Novel Class of Antifungal Agents: Current Advances and Future Perspectives. *J. Agric. Food Chem.* **2018**, *66*, 11209−11220.
(109) Franklin, N. M.; Rogers, N. J.; Apte, S. C.; Batley, G. E.; Gadd, G. E.; Casey, P. S. Comparative Toxicity of Nanoparticulate ZnO, Bulk ZnO, and $ZnCl_2$ to a Freshwater Microalga (*Pseudokirchneriella subcapitata*): The Importance of Particle Solubility. *Environ. Sci. Technol.* **2007**, *41*, 8484−8490.
(110) Pelaz, B.; del Pino, P.; Maffre, P.; Hartmann, R.; Gallego, M.; Rivera-Fernández, S.; de la Fuente, J. M.; Nienhaus, G. U.; Parak, W. J. Surface Functionalization of Nanoparticles with Polyethylene Glycol: Effects on Protein Adsorption and Cellular Uptake. *ACS Nano* **2015**, *9*, 6996−7008.
(111) Arciniegas-Grijalba, P. A.; Patiño-Portela, M. C.; Mosquera-Sánchez, L. P.; Guerrero-Vargas, J. A.; Rodríguez-Páez, J. E. ZnO Nanoparticles (ZnO-NPs) and their Antifungal Activity Against Coffee Fungus *Erythricium salmonicolor*. *Appl. Nanosci.* **2017**, *7*, 225−241.
(112) Li, J.; Sang, H.; Guo, H.; Popko, J. T.; He, L.; White, J. C.; Parkash Dhankher, O.; Jung, G.; Xing, B. Antifungal Mechanisms of ZnO and Ag Nanoparticles to *Sclerotinia homoeocarpa*. *Nanotechnology* **2017**, *28*, 155101.
(113) Perczyk, P.; Wójcik, A.; Wydro, P.; Broniatowski, M. The Role of Phospholipid Composition and Ergosterol Presence in the Adaptation of Fungal Membranes to Harsh Environmental Conditions−Membrane Modeling Study. *Biochim. Biophys. Acta, Biomembr.* **2020**, *1862*, 183136.
(114) Jeong, J.; Kim, S.-H.; Lee, S.; Lee, D.-K.; Han, Y.; Jeon, S.; Cho, W.-S. Differential Contribution of Constituent Metal Ions to the Cytotoxic Effects of Fast-dissolving Metal-oxide Nanoparticles. *Front. Pharmacol.* **2018**, *9*, 15.
(115) Jayarambabu, N.; Venkatappa Rao, T.; Rakesh Kumar, R.; Akshaykranth, A.; Shanker, K.; Suresh, V. Anti-hyperglycemic, Pathogenic and Anticancer Activities of *Bambusa arundinacea* Mediated Zinc Oxide Nanoparticles. *Mater. Today Commun.* **2021**, *26*, 101688.
(116) D'Souza, J. N.; Nagaraja, G. K.; Meghana Navada, K.; Kouser, S.; Nityasree, B. R.; Manasa, D. J. An Ensuing Repercussion of Solvent Alteration on Biological and Photocatalytic Efficacy of *Emilia sonchifolia* (L.) Phytochemicals Capped Zinc Oxide Nanoparticles. *Colloids Surf., A* **2021**, *627*, 127162.
(117) Es-haghi, A.; Soltani, M.; Karimi, E.; Namvar, F.; Homayouni-Tabrizi, M. Evaluation of Antioxidant and Anticancer Properties of Zinc Oxide Nanoparticles Synthesized using *Aspergillus niger* Extract. *Mater. Res. Express* **2019**, *6*, 125415.
(118) Ramesh, P.; Saravanan, K.; Manogar, P.; Johnson, J.; Vinoth, E.; Mayakannan, M. Green Synthesis and Characterization of Biocompatible Zinc Oxide Nanoparticles and Evaluation of its Antibacterial Potential. *Sens. Bio-Sens. Res.* **2021**, *31*, 100399.
(119) Song, W.; Zhang, J.; Guo, J.; Zhang, J.; Ding, F.; Li, L.; Sun, Z. Role of the Dissolved Zinc Ion and Reactive Oxygen Species in Cytotoxicity of ZnO Nanoparticles. *Toxicol. Lett.* **2010**, *199*, 389−397.
(120) Wingett, D.; Louka, P.; Anders, C.; Zhang, J.; Punnoose, A. A Role of ZnO Nanoparticle Electrostatic Properties in Cancer Cell Cytotoxicity. *Nanotechnol., Sci. Appl.* **2016**, *9*, 29−45.
(121) Hariharan, R.; Senthilkumar, S.; Suganthi, A.; Rajarajan, M. Synthesis and Characterization of Doxorubicin Modified ZnO/PEG Nanomaterials and its Photodynamic Action. *J. Photochem. Photobiol., B* **2012**, *116*, 56−65.
(122) Jose, A.; Sunaja Devi, K. R.; Pinheiro, D.; Lakshmi Narayana, S. Electrochemical Synthesis, Photodegradation and Antibacterial Properties of PEG Capped Zinc Oxide Nanoparticles. *J. Photochem. Photobiol., B* **2018**, *187*, 25−34.

https://doi.org/10.1021/acsomega.1c05324
ACS Omega 2022, 7, 1914−1933